IOP Publishing Journal of Neural Engineering
J. Neural Eng. **5** (2008) 232–253 doi:10.1088/1741-2560/5/2/014

On the use of musculoskeletal models to interpret motor control strategies from performance data

Ernest J Cheng[1] **and Gerald E Loeb**

Department of Biomedical Engineering, University of Southern California, 1042 Downey Way, DRB-B8, Los Angeles, CA 90089-1112, USA

E-mail: gloeb@usc.edu

Received 22 January 2008
Accepted for publication 1 May 2008
Published 27 May 2008
Online at stacks.iop.org/JNE/5/232

Abstract
The intrinsic viscoelastic properties of muscle are central to many theories of motor control. Much of the debate over these theories hinges on varying interpretations of these muscle properties. In the present study, we describe methods whereby a comprehensive musculoskeletal model can be used to make inferences about motor control strategies that would account for behavioral data. Muscle activity and kinematic data from a monkey were recorded while the animal performed a single degree-of-freedom pointing task in the presence of pseudo-random torque perturbations. The monkey's movements were simulated by a musculoskeletal model with accurate representations of musculotendon morphometry and contractile properties. The model was used to quantify the impedance of the limb while moving rapidly, the differential action of synergistic muscles, the relative contribution of reflexes to task performance and the completeness of recorded EMG signals. Current methods to address these issues in the absence of musculoskeletal models were compared with the methods used in the present study. We conclude that musculoskeletal models and kinetic analysis can improve the interpretation of kinematic and electrophysiological data, in some cases by illuminating shortcomings of the experimental methods or underlying assumptions that may otherwise escape notice.

(Some figures in this article are in colour only in the electronic version)

1. Introduction

In the absence of a rigorous understanding of the mechanics of a given experiment, interpretations of recorded data may be ambiguous. This is especially true in the field of motor control, where disagreements on the intrinsic properties of muscle have led to conflicting interpretations of many findings. A familiar example is the much-debated 'equilibrium-point' hypothesis (Asatryan and Feldman 1965). This theory depends on the intrinsic properties of muscles, including their mechanical impedance at different velocities, lengths and activation levels, their normal and reflexive recruitment, their skeletal actions and their recorded electromyographic (EMG) activity (for review, see Feldman *et al* (1998)). In particular, the viscoelastic properties of active muscles have been invoked as alternative explanations for behaviors otherwise ascribed to reflexes (Gottlieb 1998, Jaric *et al* 1998). Assumptions about the intrinsic mechanical properties of muscle also affect the interpretation of motor cortical commands (Todorov 2000). The present study tests the hypothesis that a biomechanical model with realistic muscle and tendon properties can be used to resolve such questions.

Neurophysiologists have long sought a way to understand the functional importance of various classical reflex responses to perturbations. Experimental designs have been developed that attempt to isolate the effects of reflexes from intrinsic muscle impedance. These include elimination of proprioceptive feedback by cutting off the blood supply to the

[1] Current address: Sapient Corporation, 200 West Adams, Ste. 2700, Chicago, IL 60610, USA.

muscles (Marsden *et al* 1972), comparing matched EMG traces with and without perturbations (Bennett *et al* 1994) and using sinusoidal perturbations at a frequency for which the reflex is out-of-phase as a result of neural delays (Bennett 1994). While ingenious, these methods have clear limitations: the first two methods are limited by the ability of the subject to reproduce identical movements in many subsequent trials, while the last method would be sensitive to the differential modulation of components of the reflex with different latencies (e.g., M1, M2 and M3 bursts; Lee and Tatton 1982). Mathematical models avoid the problem of inter-trial variability because they can be used to estimate the relative contributions of muscle properties and reflex responses in a single trial. This is particularly helpful when trying to tease apart the various mechanisms underlying the gradual acquisition of a motor skill, during which subjects may be changing many elements of their strategies at different rates.

Functional anatomists and biomechanists need to understand the individual roles of the various muscles that appear to have redundant actions at a given joint. Typically they have used various optimization criteria, such as minimal muscle torque or minimal muscle stress, in order to predict which muscles will be active for a given movement (e.g., Kaufman *et al* (1991), van der Helm (1994) and Chan and Moran (2006)). These analyses tend to be dominated by the relative moments of the muscles, which represent only one aspect of their architecture (Buchanan *et al* 1989), although more detailed musculoskeletal models are starting to become available (Chan and Moran 2006, Song *et al* 2008a). These optimization criteria typically ignore factors such as the effects of ligaments and tendons, the role of antagonistic muscles (Collins 1995) and the different properties of various muscle fiber types, all of which could be accounted for in a musculoskeletal model with sufficient detail. Furthermore, these and other muscle function studies (e.g. van Bolhuis and Gielen (1997)) are usually validated by correlating the preferred movements for each muscle with the EMG observed during these movements. While this provides information about the timing of motoneuronal recruitment, it does not provide reliable information about the mechanical contribution of the muscle to the movement (van der Helm 1994). Relative contributions of different muscles cannot be assessed quantitatively from EMG alone.

A final issue concerns the interpretation of recorded EMG signals. Because EMG is often assumed to represent an underlying neural activation command (e.g., Gottlieb (1996)), the quality and completeness of the recorded EMG is critical. It is rare to obtain EMG from all of the muscles that cross each joint under study. Skin surface or superficially implanted EMG electrodes tend to sample selectively from more superficial and often atypically fast-twitch, late recruited motor units (Loeb and Gans 1986, Chanaud *et al* 1991); in this case, recorded EMG may be negligible even when a significant part of the muscle has been recruited. This suggests the need for some way to assess whether the recorded EMG activity can account reasonably for the observed behavior. If recorded EMG envelopes reflect accurately and completely the muscle activation that produced the behavior, it should be possible to use the musculoskeletal model to simulate the observed kinematics. While agreement between simulated and observed behavior cannot be construed as a definitive validation, a striking disparity would provide a means to assess the nature and magnitude of deficits in the EMG data and to suggest caution in the interpretation of specific results.

Our goal was to demonstrate the utility of an accurate musculoskeletal model in understanding and quantifying the issues discussed above. We constructed a single degree-of-freedom model of the *Macaca mulatta* forearm, with eight realistic musculotendon elements corresponding to each major flexor and extensor muscle acting on the elbow. The activation of each musculotendon element was driven by the EMG activity recorded by chronically implanted electrodes in a *Macaca mulatta* performing a pointing task. We introduced stochastically predictable torque perturbations in order to test the ability of the model-based analysis to assess the evolving behavioral strategies of the monkey. Accuracy of the model was assessed initially by linearly scaling each EMG-activation input to the model to best fit the kinematic data from the elbow. Only one scalar must be fit for each muscle from a large data set including a large number of diverse movements and the corresponding EMG envelopes. We then simulated the animal's arm movements with EMG data sampled from periods corresponding to variations in presumed movement strategies, to better understand the cause of each of these adaptations. We have focused on four questions: (1) the compatibility of recorded EMG with the observed movement kinematics, (2) differential recruitment of synergistic elbow flexors, (3) use of different movement speeds to counteract anticipated perturbations and (4) the relative mechanical effectiveness of reflexes and reflex modulation. The limited results presented here are not intended to identify general motor strategies but rather to illustrate the potential value of model-based analyses of muscle torque production, impedance and energy consumption.

2. Materials and methods

Intramuscular EMG electrodes were used to record activity in eight selected elbow joint muscles during a single-joint pointing task performed by a head-restrained *Macaca mulatta* monkey. Muscle activity was recorded during time-limited, precision elbow movements that were made toward a target signified by illuminating a light emitting diode (LED; figure 1(B)), in the presence of brief torque pulses that either assisted or resisted the movement of the arm to the target according to a pseudo-random schedule. Elbow angle, tangential acceleration and external torque were recorded; elbow velocity and net muscle torque were computed. EMG data were used to drive a biomechanical model of a *Macaca mulatta* single degree-of-freedom elbow joint. The model was based on morphometric data obtained in a series of cadaver dissections (Cheng and Scott 2000).

2.1. Animal preparation

The experiment was performed at Queen's University, Kingston, Ontario, Canada, using a male rhesus monkey

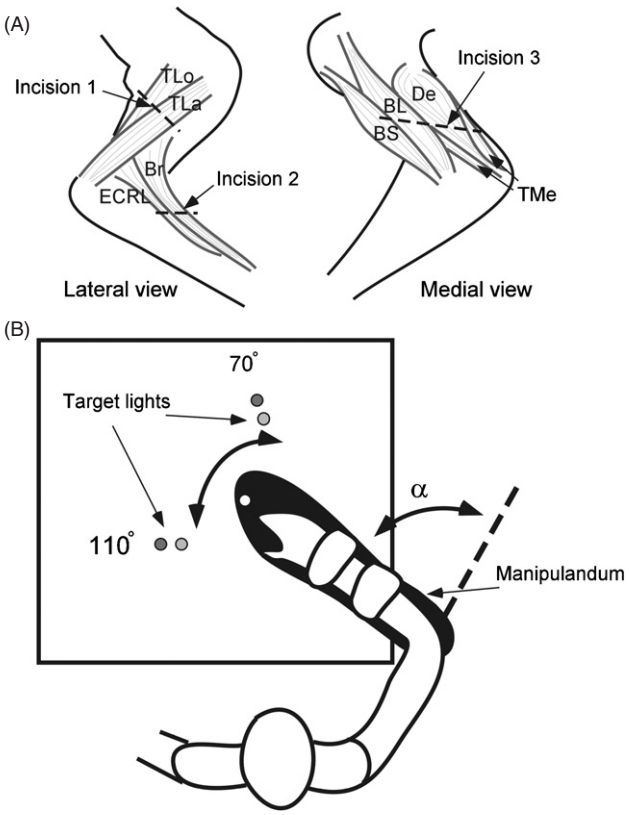

Figure 1. Experimental preparation. (A) Right arm of *Macaca mulatta* showing the placement of incisions and EMG electrodes (see the materials and methods section for abbreviations). (B) Apparatus. The animal's forearm was strapped to a manipulandum that pivoted about the elbow joint and restricted pronation/supination and varus/valgus movements of the wrist. The task required the subject to point and hold at targets at 70° or 110° (±3°) alternately, where 0° represents full extension. A green LED indicated which target was currently active and a red LED indicated when the arm was within that target window. Part way through the movement, brief torque perturbations could be applied either to assist or resist the ongoing movement.

weighing approximately 10 kg, cared for in compliance with guidelines of the Canadian Council on Animal Care. After training on the behavioral paradigm (see below), the monkey was chronically implanted with EMG electrodes and a skull pedestal; the latter allowed head fixation and incorporated a connector to the EMG electrodes. Anesthesia was induced with intramuscular ketamine HCl (10 mg kg^{-1}) followed by intravenous Saffan (0.5 ml kg^{-1}) and maintained during surgery with 1–2% isofluorane gas administered by an endotracheal tube. Heart rate, respiration rate and body temperature were monitored. Post-operative medications included penicillin, buprenorphine (analgesic) and Banamine (anti-inflammatory).

EMG electrodes were surgically implanted in the monkey's right arm under direct observation (see figure 1(A)). Incision 1 (lateral) allowed implantation of the lateral and long heads of the triceps (TLa and TLo). The extensor carpi radialis longus (ECRL) and brachioradialis (Br) muscles were implanted via incision 2 (radial side of the forearm). The short and long head of the biceps (BS and BL), medial head of the triceps (TMe) and the dorsoepitrochlearis (De) muscle were implanted via incision 3 (medial). The electrodes implanted were bipolar suture-type electrodes (Loeb and Gans 1986), with each pole made by stripping the distal 3 mm from Teflon-coated, multi-stranded, stainless-steel wire (AS-631; Cooner Wire, Chatsworth, CA). The two bared wire ends were tied together with a square knot of suture (Ethibond 3-0) in a staggered configuration such that the bared ends were 6 mm apart. They were dragged into the muscle by the suture and tied loosely so that the two contacts were oriented parallel with the fascicles. The EMG leads were passed subcutaneously to a sagittal incision across the vertex of the skull. A skull pedestal was built up from dental acrylic anchored by stainless-steel screws. It incorporated a bracket for fixing the head during the experiments and a multipin connector to which the ends of the EMG leads were soldered.

Behavioral training and data collection resumed 1 week after surgery and continued for approximately 6 months of daily sessions. After termination of the experiment, the location of each implanted EMG electrode was confirmed by autopsy. In fact, two of the eight electrodes were apparently incorrectly implanted. The electrode intended for the triceps medial head was actually recovered from the medial portion of the triceps long head, near the interface between the medial and long heads of the triceps. The electrode intended for the extensor carpi radialis longus was recovered from extensor carpi radialis brevis.

2.2. *Behavioral paradigm*

For all behavioral training and recording sessions, the monkey was seated in a custom-designed chair with its head fixed in a natural, midline posture. The monkey's right forearm was strapped to a pivoting arm manipulandum which had its center of rotation aligned with the elbow joint (figure 1(B)). The position of the trunk was controlled to minimize the use of shoulder or trunk muscles. The arm posture was similar to that used in most horizontal planar arm movement tasks (e.g., Georgopoulos (1986)), with the upper arm abducted about 70° with respect to the trunk. The subject worked in a darkened room to reduce distractions, but could be monitored by an infrared video camera. Throughout the workspace the animal had a clear view of an illuminated orange LED at the tip of the manipulandum aligned approximately with its index finger.

The animal's task was to flex and extend its forearm such that the orange LED pointed to one of two green target LEDs fixed to the table at 110° and 70° elbow flexion, respectively, and to hold at that position until instructed to move again. Alongside each green target LED there was a red status LED (R1 and R2) that designated when the arm was aligned within the target window (typically ±3°). If the movement overshot the target window or took longer than the allotted time, both LEDs turned off momentarily to indicate an error. Before the next trial could begin, the arm had to be held in the target window for a randomized hold period (0.5–1s) to prevent anticipation. The current target and status LEDs were then extinguished and the other green target LED was

illuminated. Correct trials were signaled by an audible tone and the rewarding of the animal with a small amount of water to reinforce the correct behavior. Incorrect trials were signaled by blinking off the green and red LEDs and by withholding the water reward. To ensure that the subject was motivated in the task, water bottles were removed from the monkey's home cage 24 h prior to any experimental session. Body weight and general health were monitored daily to safeguard the well-being of the animal. The animal was given water and fruit ad libitum after the recording session.

During each movement sequence, the manipulandum passed through a predefined 'torque window' at 25% of the requested excursion to the illuminated target. At this point, a 10 ms torque pulse (APEX 40 Compumotor; Parker Hannafin Corp., Rohnert Park, CA) could be applied to perturb the movement. The direction of the torque pulse was defined as assistive if it acted in the direction of the movement underway or resistive if it acted to oppose the movement. The amplitude of the torque pulse was selected such that it altered the success rate of the task initially (necessitating a change in movement strategy in order to receive rewards) but still permitted the animal to develop a strategy that was successful for most trials. Actual torque amplitude was increased gradually from 0.8 N · m during initial training sessions to 1.62 N·m during later sessions. The probability of each type of perturbation (unperturbed, resistive or assistive) was pre-specified for each block of 150–200 trials. Consecutive blocks with differing probabilities could be given without interruption to look at the process of modifying the strategy as the animal became aware of the changed probability.

In a given experimental session, the subject generally started with around 20 unperturbed trials in each direction. This served two purposes: first, to re-familiarize the animal with the task, and second to allow the muscle to 'warm-up' and reach a potentiated state. It has been shown that muscle contractile properties are significantly different before potentiation (Brown and Loeb 1999). The duration of a session (typically 60 min) was limited by the attention span of the animal rather than any apparent muscle fatigue.

2.3. Data collection

EMG signals were differentially amplified (ACamp; AC Instruments Inc., Seattle, WA), bandpass filtered (100 Hz–2 kHz), full-wave rectified and integrated into discrete 2 ms bins (Pulsed Sample/Hold Integrator PSI-1, Bak Electronics, Mt. Airy, MD; Bak and Loeb 1979) that were digitized synchronously with the clock to this bin integrator. Angular position was measured by a potentiometer in the rotating joint of the manipulandum, and an accelerometer measured tangential acceleration at the distal end of the manipulandum. Vertical and horizontal forces were measured by strain gauges affixed to the manipulandum between the arm cast and the rotor of the torque motor. Control of LEDs, torque perturbations and rewards, on-line monitoring of data collection and storage of data for later analysis were performed by a Pentium PC using real-time data acquisition software (REX; Hays *et al* 1982). Data from each trial were collected from 200 ms preceding initiation of the movement to 100 ms following either an error signal (i.e. overshooting the target window or exceeding allotted time) or successful completion of the movement and hold. Data were analyzed in Matlab (Mathworks, Natick, MA). EMG signals were smoothed with a 10 ms moving average window and baseline noise was subtracted. For some analyses, EMG data from multiple trials were averaged after aligning the records at the time at which the manipulandum entered the torque window.

In order to compare movements made at different speeds, we measured the elbow velocity that occurred at the time of peak acceleration. This epoch tended to occur between −30 and −20 ms relative to the torque window for most trials. Peak velocity was not analyzed because it tended to occur roughly 50 ms after the torque window, when it might have been modified by a perturbing torque. Peak acceleration was tightly correlated with peak velocity when unperturbed trials were examined.

2.4. Quantification of reflex component of EMG

To examine changes in reflex modulation, average EMG activity during the reflex epoch was quantified. This epoch was defined as the period of time from 10 to 100 ms after perturbation onset. This window was chosen because the shortest-latency reflexes (M1) in monkeys were shown to occur at a latency of 10–12 ms after perturbation (Lee and Tatton 1975), while voluntary responses occurred after 100 ms (e.g., Nakazawa *et al* (1997)). Changes in the background level of activity in a motor pool can produce changes in the magnitude of the recorded reflexive EMG activity even if the synaptic input responsible for the reflex does not change (Stein and Capaday 1988). Therefore, EMG activity between −80 and 0 ms was also averaged. The epoch during the possible torque pulse was not analyzed because of the possibility of electrical artifacts from the torque motor.

The modulation of reflex epoch EMG activity was examined only in the medial region of triceps long head (TMeLo) for two reasons. Its signal appeared to be most representative of the whole muscle's activity (see musculoskeletal model design below and the discussion section), and it produced the largest long-latency reflex response (i.e., M2 and M3 response latencies, typically occurring 50:80 and 80:100 ms after perturbation, Yamamoto and Ohtsuki 1989). The latter point is important because M2 and M3 reflexes may be associated with a supraspinal pathway (Lee and Tatton 1975, Marsden *et al* 1972) and have been shown to be modulated according to the task performed (Nakazawa *et al* 1997); thus, a change in this activity is most likely to reflect an adaptive strategy. While studies have shown that short-latency, M1 responses can be modulated, these changes require weeks to appear (Wolpaw *et al* 1994).

Changes in movement and muscle activity were examined within a single session and also over many sessions. General trends were determined by applying a moving average to the measured parameters. Values were also grouped based on the type of perturbation applied during that trial; for example, all extension-direction, resistive-perturbation trials in a single session were grouped and analyzed for extensor reflexes.

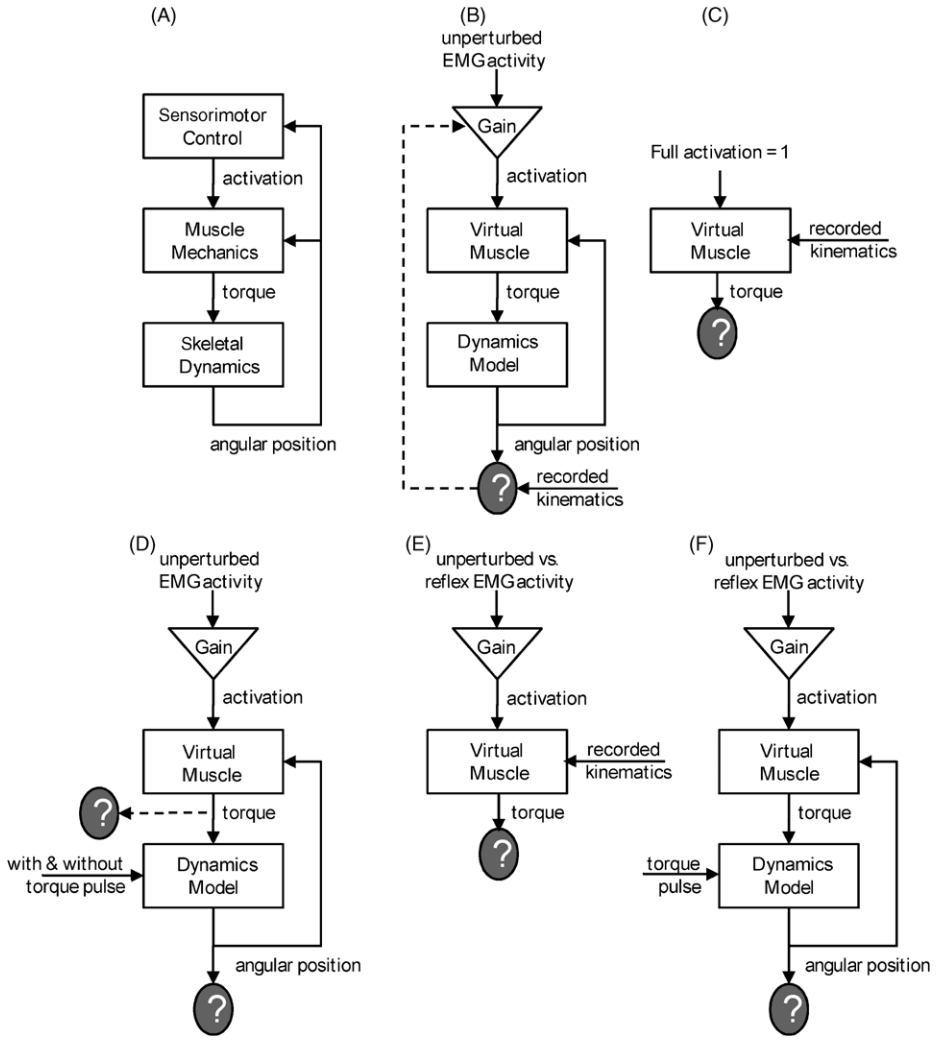

Figure 2. (A) Schematic representation of the *general hierarchy* of physiological processes and the models used to study them. Muscle torque drives the forearm skeletal dynamics resulting in changes in the angle of the forearm that are fed-back to both higher levels. For example, joint angle and velocity affect the force–length and force–velocity relationships in muscle mechanics and contribute sensory feedback that may generate reflexive changes in activation. (B) To *calibrate the model*, EMG signals from unperturbed trials were scaled linearly to drive activation of the muscles. The scaling factor was adjusted iteratively to minimize the sum of the squared differences between position at the termination of the simulation compared to experimental data (see figure 5). (C) To *compute the maximal torque* that each muscle could contribute to the task, its kinematics were set to the experimentally observed trajectory and activation was set to maximal (see figure 6). (D) To examine *effects of intrinsic muscle impedance* without reflexes, EMG from unperturbed trials was used both with and without perturbations, with changes in torque and kinematics being compared (see figure 3). (E) To quantify the *effectiveness of reflexes in individual muscles*, we compared the muscle torques produced by activation derived from EMG recorded during unperturbed versus perturbed trials (see figure 4) while driving the kinematics with the recorded arm trajectories. (F) To determine the *effects of reflexes on overall task performance*, we evaluated the kinematics produced by the unperturbed and perturbed activation patterns (see figure 11).

2.5. Musculoskeletal model design (figure 2(A))

A musculoskeletal model of the *Macaca mulatta* arm was constructed to simulate the performance of the task by the subject monkey. The elbow was modeled as a single degree-of-freedom joint; supination/pronation torque was ignored as it was unnecessary for this task and such motion was prevented by the cast. The model was constructed using Matlab 5.3 and its associated simulation module, Simulink 3.0 (Mathworks, Natick, MA). The model consists of a segment dynamics element that describes the motion and inertial properties of the forearm and muscle/torque-generating elements that are driven by the eight recorded EMG signals. The general structure is based on a hierarchical model of motor control consisting of three levels (figure 2(A); Loeb *et al* 1999). The configuration of model inputs and outputs varied depending on the question being addressed; specific configurations are described later. The highest level (sensorimotor) generates the input signals (either the recorded EMG data or preset values) that drive the muscle mechanics model. The kinematics of the forearm drive the length of each musculotendon element; these data are obtained from the recorded joint angle or fed-back from the model of skeletal dynamics at the lowest level of the

Table 1. *Macaca mulatta* muscle morpohometry used to create the elbow joint model. Positive moment arm indicates that muscle acts in the flexion direction, while negative moment arm indicates extension direction.

Muscle name	Abbr	Muscle mass (g)	Fascicle L_0 (cm)	Tendon L_0^T (cm)	Pennation angle (°)	Moment arm (cm)
Brachialis	B	19.7	4.3	2.9	–	1.5
Brachioradialis	Br	24.2	11.1	3.6	–	3.5
Biceps long head	BL	35.1	5.4	8.8	–	3.2
Biceps short head	BS	22.0	6.6	5.7	–	2.5
Extensor carpi radialis longus	ECRL	13.1	5.7	10.0	–	2
Dorsoepitrochlearis	De	11.9	5.8	4.4	–	−1.35
Triceps lateral head	TLa	44.7	4.3	9.3	21	−1.8
Triceps long head	TLo	25.5	3.8	9.5	31	−2.15
Triceps medial/long head	TMeLo	47.6	4.2	3.2	18	−1

hierarchy. The skeletal dynamics model accepts and sums the muscle forces, converts them to signed torques (positive forces corresponding to flexion- and negative forces to extension-direction torque) and computes the kinematics of the forearm based on the rotational inertia:

$$\alpha = \tau_{\text{total}}/I_{\text{forearm}} = (\tau_{\text{muscles}} + \tau_{\text{perturbation}})/I_{\text{forearm}} \quad (1)$$

where α is the angular acceleration of the forearm segment, τ is the torque about the elbow joint (torque in the flexion direction is assigned a positive value) and I is the inertia. Inertia of the forearm was calculated by summing inertia about the axis of rotation for both the animal's forearm and hand and the manipulandum/torque motor rotor. Inertia of the forearm and hand was predicted using a regression based on the length of each segment and the animal's total mass (Cheng and Scott 2000). The total torque acting on the forearm consists of that produced by the muscles (active plus passive tension times moment) plus experimentally applied torque pulses used to perturb the voluntary movement. Note that this analysis ignores viscoelastic properties of the skin and joint, which were not available but are often assumed to be negligible for such proximal joints operating near the middle of their range of motion.

The muscle + tendon models consisted of Simulink blocks created by a Matlab modeling software package called Virtual Muscle (Cheng *et al* 2000). See table 1 for specific values describing the morphometry and contractile properties of each muscle (derived from Cheng and Scott (2000)). Each block requires length and activation as inputs and generates total muscle force as an output. Each muscle block consisted of three interacting elements: a contractile element with active and passive viscoelastic properties, a series-elastic element representing the tendon and aponeurosis for the muscle and a muscle mass element with inertial properties. The passive viscoelastic and series-elastic elements both act on the muscle mass to prevent instabilities from arising within the muscle. The contractile element has realistic behavior with respect to force–length, force–velocity, activation rise and fall times, yield and sag as measured and modeled in feline muscle (Brown *et al* 1999). The series-elastic element represents a lumped model that groups the tendon with the aponeurosis; this has been shown experimentally to be reasonable (Scott and Loeb 1995). The model of the tendon and the interaction between the contractile element and the tendon have been described elsewhere (Loeb *et al* 1999).

Maximal fascicle length (L_{max}) was assumed to be 1.3 times optimal fascicle length (L_0); this measure is used in the model to scale the amount of elasticity in parallel with the contractile element (Brown *et al* 1996). Muscle path lengths were set such that for elbow flexors the fascicles were at L_0 when the elbow was at 70° flexion and for elbow extensors at 110° flexion. This presumes that each muscle operated over the ascending limb of its force–length curve (Goslow *et al* 1977). These assumptions were made to attenuate passive muscle elasticity over this range; we felt this was reasonable because there is little passive tension produced by the contractile element even at L_{max} (7% of maximal isometric force [F_0], Brown *et al* 1996); in rapid, small-amplitude movements, active muscle viscosity is far more significant than passive muscle elasticity. For computational efficiency, each musculotendon element was modeled using a single feline slow-twitch fiber type (Cheng *et al* 2000). Initial testing indicated that incorporating multiple fiber types and motor units in the muscle models greatly increased simulation time but did not significantly change results in this paradigm (but see the discussion section).

Each musculotendon element acted on the segment through a fixed moment arm. This assumption appears reasonable because moment arms as measured in human elbow muscles do not change greatly over the limited range of movement modeled (Pigeon *et al* 1996). For movements from 70° to 110° in the human elbow, brachioradialis moment arm changes the most, by approximately 15%, while all other moment arms remain fairly constant. Static *Macaca mulatta* elbow muscle moment arm measures were obtained from a single animal, with the elbow at 90° flexion (see table 1).

As the muscle model itself was designed to ignore effects of pennation, some adjustments were made in the case of three muscles with significant pennation angles (i.e., over 10° (Zajac 1989, Veeger *et al* 1997)). For the three heads of the triceps, force output was scaled by the cosine of the pennation angle at 90° elbow angle to capture only the vector of force acting parallel to the line of action of the musculotendon element. Fascicle length changes from movement of the elbow joint were also scaled by the cosine of the pennation angle.

Activation of each musculotendon element was driven by recorded EMG values, normalized to a neural activation level between 0 and 1 (described in a following section). Adaptations to the model were required to deal with

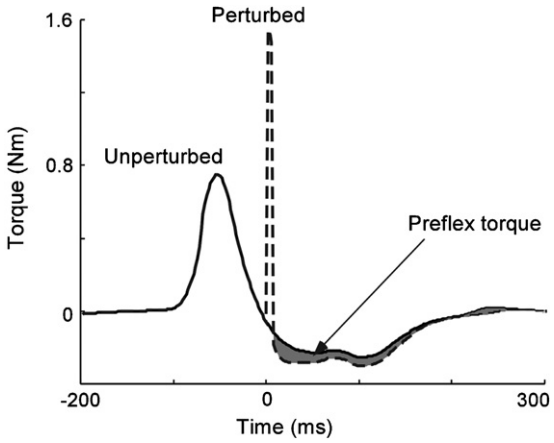

Figure 3. The mechanical impedance of the musculoskeletal system causes muscles to generate different torques when the same activation pattern is run with different kinematics (see figure 2(D)). In this example, the EMG recorded from an unperturbed trial was used to activate a muscle model operating under the unperturbed kinematic conditions (solid line) and under the perturbed kinematics (dashed line), resulting in a preflex torque difference between them (shaded region).

shortcomings in the EMG recordings. First, the triceps medial head was not properly implanted. Instead, the electrode was implanted in the medial region of the triceps long head, although it recorded distinctly different modulation of EMG from the other long head site under some circumstances (see figure 5). To account for this, the EMG signal from the misimplanted electrode was used to drive a muscle that had the morphometric properties of the triceps medial head but also included half of the PCSA of the triceps long head (this combined muscle is abbreviated as TMeLo). Second, the ECRL electrode was implanted in the extensor carpi radialis brevis (ECRB). Although ECRL is usually considered to contribute only minimally to elbow flexion (Salmons 1995), we measured a significant moment arm about the elbow joint (2.0 cm, see table 1). The EMG signal from ECRB was used to drive the model ECRL based on the assumption that they would be similarly modulated, but we do not know of any data supporting or refuting that assumption. Finally, brachialis was not implanted. In our model, brachialis was driven by the EMG signal recorded in brachioradialis; this is justified by the observation that during isometric conditions, these two muscle were shown to have linearly correlated levels of EMG activity (Buchanan *et al* 1989). The validity of these assumptions and modifications is examined later (see the discussion section).

2.6. Musculoskeletal model calibration (figure 2(B))

Recorded EMG and kinematic data were used as inputs to drive each simulation trial of the forearm movement. Activity of each musculotendon element was determined by linearly scaling the EMG envelope recorded for each muscle during the behavioral trial. Because scaling by maximal voluntary contraction (e.g., Soechting and Flanders (1997)) cannot be used in non-human subjects, we iteratively adjusted the scaling factor for each muscle independently until endpoint accuracy was maximized based on least-square residual error (e.g. figure 5(E)) for all the calibration trials from several sessions over the course of the data collection period. A single set of scaling factors was used throughout all simulation analyses. Residual discrepancies (as discussed below) were used to identify potential flaws in the recorded data and the muscle models that would otherwise be buried as untested assumptions in the interpretation of the results.

2.7. Task differentiation of synergistic muscles (figure 2(C))

To identify functional differences between apparently synergistic muscles, the maximal torque-generating capacity of each muscle during the flexion- and extension-direction movements was determined. Musculotendon elements were maximally activated, and kinematics were driven by the position signal recorded in the behavioral trials. Torque output of each muscle was simulated (see below and figure 6(B)).

2.8. Movement speed and impedance (figure 2(D))

We examined changes in energy consumption and intrinsic muscle impedance as movement speeds changed over the sessions. Simulations were run using data from the unperturbed 'warm-up' trials from each session, thus isolating intrinsic muscle viscoelasticity from any reflex effects (see below and figure 3). These trials were chosen to represent changes in the 'default' strategy over all sessions for three reasons. First, because data were recorded before the first perturbations for that session, these data were indicative of the long-term strategy adaptations acquired by the animal, as opposed to adaptations specific to the varying blocks of perturbation types within a session. Second, we hoped to avoid inconsistencies resulting from the independent changes in EMG and force with fatigue (Bigland-Ritchie *et al* 1983). Finally, the motivation of the animal often declined throughout a session; performance and error rates later in a session could become inconsistent.

To compute muscular energy consumption, we applied the function used previously in Loeb *et al* (1999), which is adapted from Schutte *et al* (1993). Briefly, the energy consumed by the two muscles is based on the mechanical power generated by the muscles and the heat generated by the muscles. The heat generated is based on the sum of the maintenance heat and the heat generated by shortening and lengthening of the muscle.

$$h = (0.7c_h\mathrm{FL}(L) + 0.3c_h)^*\mathrm{act}^*R + \begin{cases} -\alpha^*V^*\mathrm{FL}(L)^*\mathrm{act}^*R, \text{ when } V \leqslant 0.204 \\ (0.35V - 0.035)\mathrm{FL}(L)^*\mathrm{act}^*R, \text{ otherwise} \end{cases} \quad (2)$$

where c_h is a constant, determined to be 0.07, FL(L) is the normalized force–length curve, act is the muscle activation, R is the recovery heat constant, determined to be 2.5, α is a constant, determined to be 0.16 + 0.18 Factive (muscle) and V is the velocity of the muscle normalized to units of optimal fascicle length (L0 s^{-1}).

Intrinsic muscle impedance, i.e. 'preflexes' (Brown and Loeb 2000b), were quantified by finding the difference between torque produced following a perturbation and the nominal torque produced with the same muscle activation

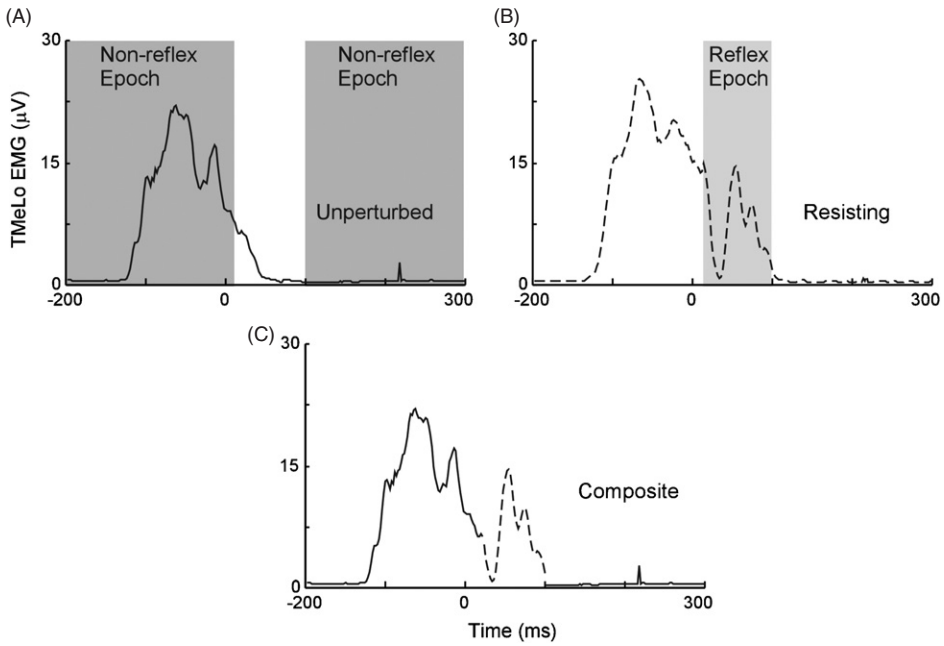

Figure 4. Technique used to isolate the effects of reflex-induced EMG. (A) EMG recorded from TMeLo in an unperturbed trial was combined with (B) EMG from the same muscle but with a perturbation applied. (C) The composite of the two records used the EMG from the non-reflex epochs in the unperturbed trial and the reflex-epoch in the perturbed trial (shaded portions in (A) and (B)). This technique was used to minimize the effects of variability between trials and to eliminate the effects of any voluntary responses.

pattern but without a perturbation (figure 3). This torque measure has been labeled a 'preflex torque'. In this example, the torque pulse assisted the flexion movement being produced voluntarily. The preflex has a net extensor effect resulting from the reduced torque of the more rapidly shortening flexors plus the increased torque of the more rapidly stretched extensors.

2.9. Contribution of reflexes to controlling perturbations (figures 2(E), 2(F) and 4)

Torque output was compared from simulations driven by EMG from unperturbed and perturbed trials to assess the effects of reflex-induced EMG. Kinematics were from data recorded in unperturbed trials. Activation for perturbed simulation trials was derived from a composite of EMG activity from the unperturbed trials substituted during the reflex epoch (10:100 ms) by the EMG levels from perturbed trials (see figure 4 and below). This technique was used to eliminate any changes in prestimulus activation as a result of exposure to the perturbations and to remove the effects of any post-stimulus voluntary adjustments, which occur with a minimal latency of 100 ms (e.g., Nakazawa *et al* (1997)). No perturbation was applied during these simulations, as the intent was to assess changes in torque produced only by reflex EMG responses, not preflexes. The contributions of reflexive EMG independent of any preflexes was taken to be the difference between torque produced during the simulation of unperturbed and unperturbed/perturbed composite EMG (in fact, the kinematics of the actual perturbed trajectory result in somewhat different reflex torques).

The effects of reflex-induced EMG responses on arm endpoint trajectories were also examined in the presence of perturbations. As above, unperturbed and composite unperturbed/perturbed activation was used. Musculotendon lengths were fed-back from simulated kinematics (figure 2(F)). Any difference between trajectories simulated with unperturbed and unperturbed/perturbed composite EMG was attributed to the contributions of reflexes.

3. Results

3.1. Estimating muscle torques from recorded EMGs (figure 5)

The force calibration method described above was used to predict the torque produced by each muscle individually. Averaged EMG and kinematic data illustrated in figure 5 are characteristic of sessions later in the data collection period (approximately session 15 and on); the earlier trials are discussed in a following section. Note that while only eight EMG signals were recorded, a total of nine muscles were simulated; this is because muscle activity recorded from brachioradialis was also used to drive the modeled brachialis muscle. The net predicted torque is proportional to the predicted acceleration (figure 5(C), solid lines). Integrating once produces the predicted velocity (figure 5(D)) and again yields position (figure 5(E)). Qualitative discrepancies between predicted and observed kinematics were particularly large during periods of positive (flexor) acceleration in both tasks. The velocity and position

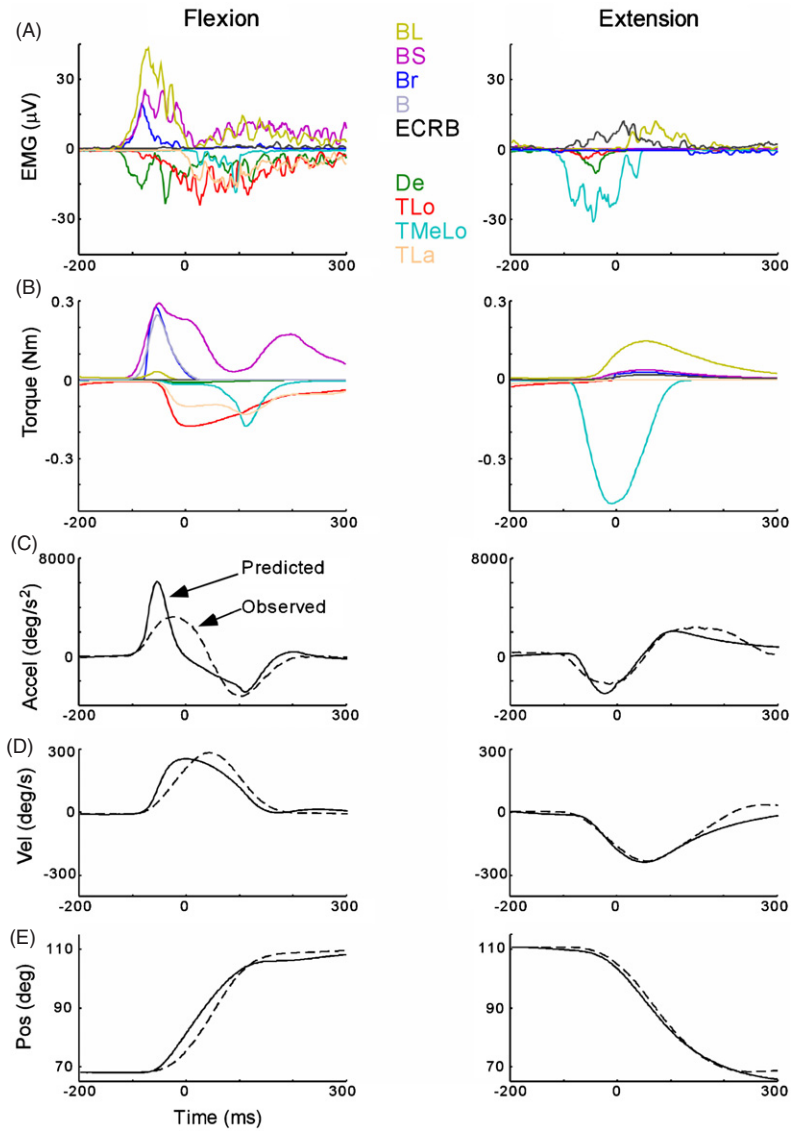

Figure 5. Calibration of musculoskeletal model for flexion- (left column) and extension-direction (right column) movements. (A) Averaged EMG signals for each muscle (extensor muscle EMGs and torques shown as negative values), which were then scaled by an optimized set of gains to generate activation signals for the muscle models (see the materials and methods section). (B) Force outputs of the muscle models were converted to torques. (C)–(E) Kinematics (acceleration, velocity and position, respectively) predicted by the model (solid lines) were compared with observed kinematics (dashed lines) to determine goodness of fit for the calibration.

trajectories show what appear to be smaller effects, but note that the calibration method forces the simulations as a whole to converge on the correct final position at zero velocity. See the discussion section and figure 13 for further analysis.

For elbow flexors used as agonists in the flexion task, well-defined EMG bursts in biceps long (BL), biceps short (BS) and brachioradialis (Br) began at −100 ms and ceased abruptly between −10 and +10 ms. Unexpectedly, acceleration of the forearm (figure 5(C), the dashed line in the left column) outlasted the EMG activity by 70–90 ms; a more reasonable value based on the delay inherent in the model of muscle activation would have been 50 ms. Antagonist activity at the end of the extension task was observed primarily in BL during the interval +5 to +150 ms; BS and Br were largely quiescent during the braking phase. Deceleration at the end of extension also outlasted the elbow flexor activity by 110 ms (figure 5(C), the dashed line in the right column).

Extension movements were characterized by a lower overall level of muscle activity and lower accelerations and peak velocities. Agonist phase activity in elbow extensors appeared to involve TMeLo almost exclusively and occurred during the interval −120 ms to +20 ms. TLa and TLo showed only minimal agonist activity during the extension task, despite their strong contribution to braking the flexion movement. The extensor-ward acceleration of the forearm outlasted extensor muscle activity by only 50 ms. Braking activity by the elbow extensors at the end of the flexion task was less crisp and was accompanied by cocontraction of the flexors suggestive of a

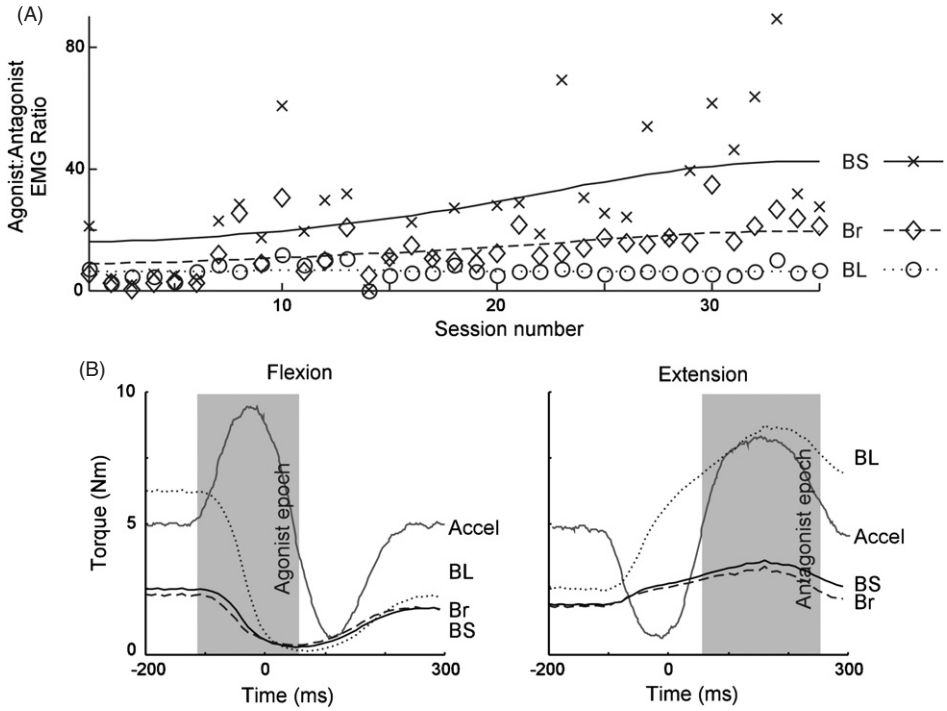

Figure 6. (A) Ratio of agonist epoch EMG activity to antagonist epoch activity for three elbow flexors versus session number. A higher ratio indicates that the muscle has a greater bias for activity during acceleration of flexion-direction movements, as opposed to during braking of extension-direction movements. BS (solid lines) and Br (dashed lines) muscles had a relatively greater bias for the acceleration task, while BL (dotted lines) had a relatively greater bias for the braking task. BS and Br bias also increased over time. (B) Predicted torque (relative to maximal isometric torque) generated by each muscle when maximally activated over the course of flexion- and extension-direction movements. Torque decreased during flexion-direction movements as muscles were shortening during the movement. BL fascicles shortened the fastest due to its architecture; consequently, the force decrease was greater. Conversely, BL fascicles lengthened fastest during extension-direction movements, thus the force increase caused by the lengthening was greatest. Positive and negative acceleration values were used to delimit the agonist and antagonist epochs, respectively (shaded regions).

triphasic burst pattern. Dorsoepitrochlearis (De) was generally active throughout the entire movement, while triceps long (TLo), triceps lateral (TLa) and triceps medial/long (TMeLo) had somewhat more phasic activity. The deceleration at the end of flexion (figure 5(C), the dashed line in the left column) outlasted the elbow extensor activity by approximately 50 ms, consistent with the fall time of the muscle model.

3.2. Task-dependent differentiation of synergistic muscles (figure 6)

Interestingly, the synergistic elbow flexors appeared to be recruited differentially depending on whether they were used in an agonist (accelerating) role or an antagonistic (braking) role. As described above (figure 5), BL, BS and Br EMG signals were strong during the agonist epoch of flexion movements, but only BL was significantly active during the antagonist epoch of extension-direction movements. These kinds of task-specific recruitment are particularly powerful constraints for the process of scaling EMGs to account for torques across all tasks. To quantify these differences in levels of activity, we computed a ratio of average agonist EMG signal (−120:70 ms in flexion trials) to the average antagonist EMG signal (50:270 ms in the subsequent extension trials) for each elbow flexor muscle. Figure 6(A) shows these ratios and trend lines for 35 successive sessions of the unperturbed tasks. The tendency toward task-dependent selective recruitment was low at first in all muscles and stayed low for BL but grew steadily in Br and BS, which decreased their contribution to braking as the animal became more practiced in the extension task.

To differentiate the functions of synergistic elbow flexors during the two directions of movement, their force producing capabilities over the course of the ballistic movement were modeled. Figure 6(B) shows the predicted force produced by each musculotendon element under constant maximal activation as the arm is driven through both flexion- and extension-direction movements. As the forearm moves in the flexion direction, the shortening of the elbow flexors reduces their force-generating capabilities as a result of both the force–length and force–velocity dependences. Conversely, as the muscles lengthen during the rapid extension movement, they are able to produce forces greater than during a maximal isometric tetanic contraction (F_0). These effects were largest in both directions for BL, whose relatively short fascicle length magnified the effects of joint angle changes at the sarcomere level. This effect can be quantified for and compared among muscles by computing the ratio of their moment arms (MA) to their fascicle lengths (Lf): BL = 3.2 cm/5.4 cm = 0.6, BS = 2.5/6.6 = 0.38, BR = 3.5/11.1 = 0.31. At the beginning of the flexion movement, all elbow flexors are able to produce an amount of force equal to their F_0, because fascicle lengths

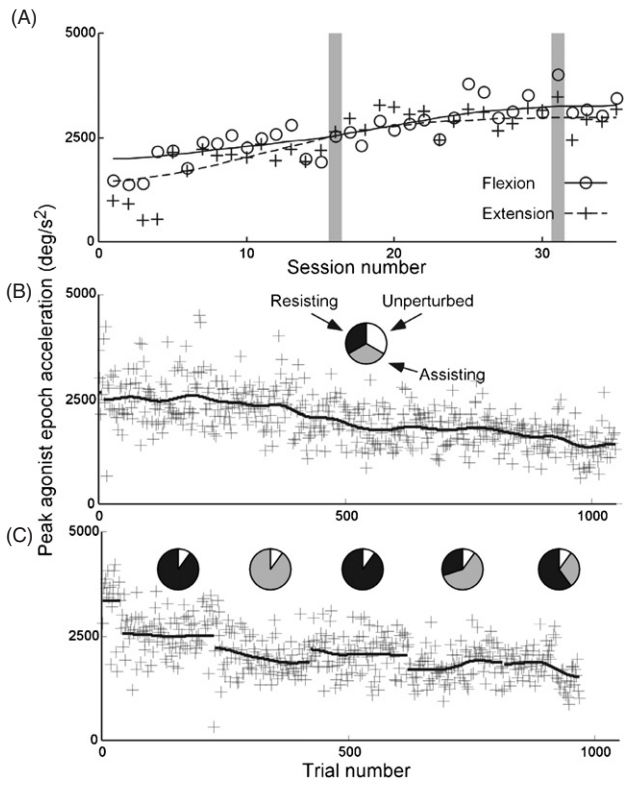

Figure 7. (A) Peak acceleration versus session number for flexion- (circles) and extension-direction (crosses) movements. Peak acceleration is used as an indication of movement speed (see the materials and methods section), which had a generally increasing trend over the study. Gray bars indicate sessions examined in greater detail below. (B) Change in peak acceleration versus trial number in session 16. Pie charts indicate the relative amounts of each perturbation type used for each block of trials within the session; black indicates the proportion of resistive perturbations, gray indicates the assistive perturbations and white indicates the unperturbed trials. This session consisted of equal amounts of each perturbation type, randomly distributed. Peak acceleration for each trial is indicated with a cross, while black lines indicate general trends for each block of trials, using a moving window average. Note decreasing peak acceleration over the course of the session. (C) Change in peak acceleration versus trial number in session 31. For the first three blocks, peak acceleration was higher in blocks with a higher percentage of resisting perturbations.

were specified to be at L_0^{M} for this joint angle. The stronger BL produces a greater initial torque than BS and Br, but as the arm begins moving and the muscles shorten, all three muscles produce similar absolute torques. At the beginning of the extension-direction movement, the muscles are shorter than their optimal lengths, an effect that is largest for BL. However, BL benefits more rapidly from the stretching motion during the extension, causing it to be a more effective brake on this phase than the other two flexors. As the monkey became more familiar with the task, he appeared to be taking advantage of this biomechanical detail to improve efficiency.

3.3. Movement speed and impedance (figure 7)

In order to determine whether 'default' movement velocity changed over time, we computed the mean peak acceleration for the 15 unperturbed 'warm-up' trials at the beginning of each of the 35 sessions (figure 7(A)). The trend lines show a gradual increase for both movement directions. Thus, before the animal was exposed to any perturbations in a given session, initial movement speeds tended to increase over time. The maximal allotted time to complete the movement did not change over these sessions, so the animal was not explicitly required to change its movement speed. Perturbation sizes did increase over time, however, so the change in movement speed may have been a learned response to cope with the increasingly strong perturbations that the monkey came to expect (see the discussion section).

In general, movement speeds decreased within individual sessions. Figure 7(B) shows the trend for session 16, which included ∼1000 trials with equal probabilities of resistive, assistive and no perturbations. Figure 7(C) shows that the monkey adjusted his strategy abruptly during session 34 when the distribution of the perturbations changed. The addition of 90% resistive perturbations at the beginning caused an immediate decrease in peak acceleration. The next shift from resistive to assistive perturbations produced a further abrupt decrease in acceleration that was reversed when the perturbations switched back to resistive; acceleration again dropped when some assistive trials were added back.

3.4. EMG activity accounts for movement speed, mechanical impedance and energy cost (figure 8)

We picked three sessions in which there were long series of unperturbed extension trials with consistent but substantially different peak velocities and accelerations. Extension movements were selected in order to avoid confounding factors related to the relatively poor fit of scaled flexor EMG data to account for flexion kinematics. The EMG records from these trials were averaged and used to drive the model arm during unperturbed and resistively and assistively perturbed simulations. The unperturbed accelerations of the forearm are illustrated in figure 8(A). The EMG data from session 1 were recorded before the animal had been exposed to perturbations for the first time; movements were not as brisk as in later sessions and EMG activity was attenuated. The larger accelerations recorded in sessions 16 and 34 were associated with higher EMG levels, which resulted in higher predicted acceleration and energy consumption (figure 8(B)).

Simulations with perturbations indicated that the higher energy strategies were more effective at minimizing the kinematic effects of the perturbations even in the absence of reflexes. Figure 8(C) shows the trajectories with and without perturbations and predicts the mean angular deviations of the perturbed trajectories at the time when the arm was expected to be in the target window (vertical gray bars at 150 ms after the perturbation window). The medium energy utilization strategy (figure 8(C), middle) from session 16 reduced the mean perturbation error from 4.95° for the low-energy strategy to 3.99°. The high-energy utilization strategy (figure 8(C), bottom) resulted in the smallest endpoint error (3.43°), almost sufficient to stay in the target window without reflex contributions. Preflex torque (computed during the

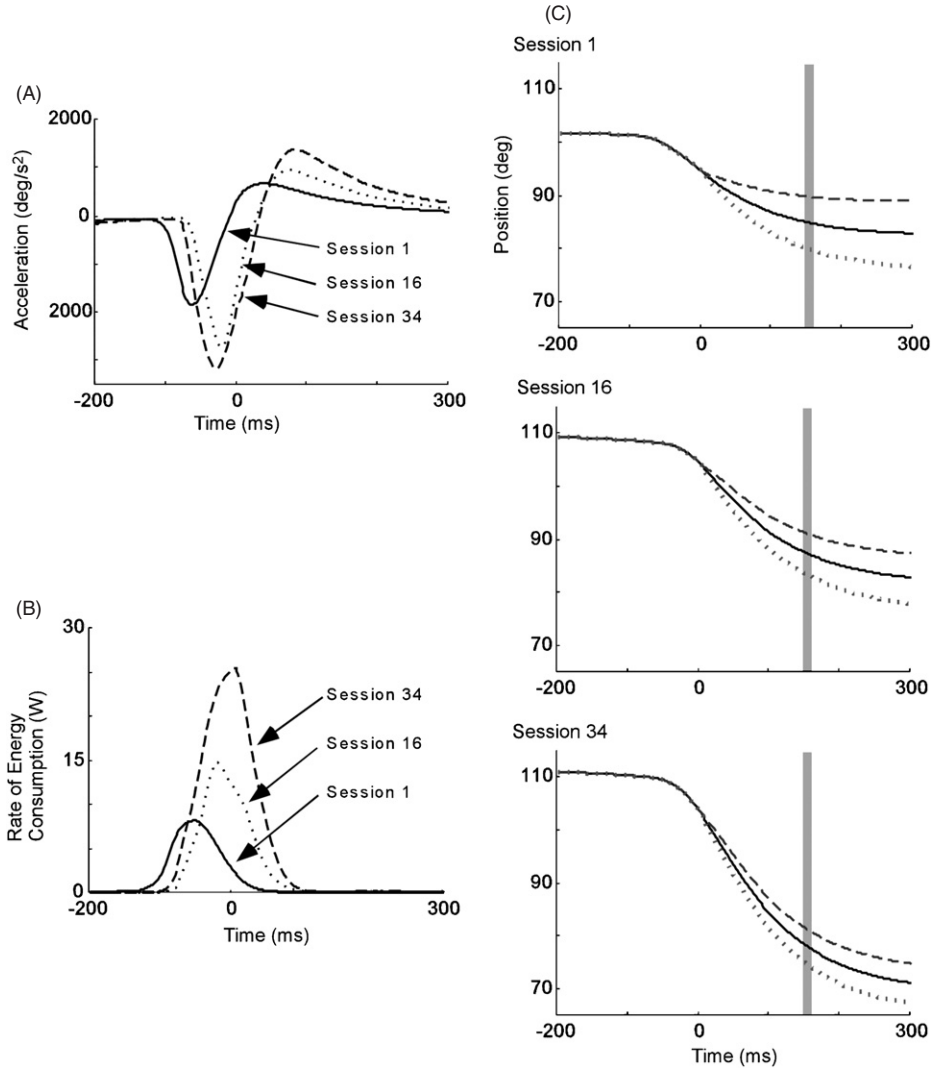

Figure 8. (A) Predicted acceleration versus time for three extension-direction trials from sessions 1 (solid lines), 16 (dotted lines) and 34 (dashed lines). Later sessions produced faster movements. (B) Energy consumption versus time for the same three sessions. The later, faster movements were more energy intensive. (C) Predicted trajectories for the same three sessions under resistive (dashed lines), assistive (dotted lines) and unperturbed (solid lines) conditions. Gray bar indicates the time when the hand entered the target window. Error is defined as the mean deviation in hand position caused by the perturbations, relative to the unperturbed trajectory at the time when the hand entered the target window. The faster, more energy intensive movements of the later sessions were affected less by the perturbations, resulting in a lower amount of error (see the text).

window 10:20 ms after the perturbation) tended to covary with energy consumption: 0.055 N m for the low-energy strategy, 0.087 N m for medium energy and 0.121 N m for high energy. (The 0:10 ms epoch could not be examined because preflex responses in this period were occluded by the perturbation torque itself.)

3.5. Preflex torque was correlated strongly with muscle torque and weakly correlated with muscle activity (figure 9)

The preflex torques arise from the intrinsic mechanical properties of the muscles, which manifest themselves according to the level of activity in the muscles. We developed four indices to summarize that activity in order to determine which correlated best with the magnitude of the preflex torque. The simulation analysis described above (figure 8) was performed using the EMG data averaged from the 'warm-up' trials for all sessions. The preflex torque was computed for both extension and flexion tasks and for assistive and resistive perturbations; values ranged from 0.02 to 0.14 N m. The activation indices were based on the sum of the calibrated activation signals, weighted by each muscle's maximal isometric force (F_0) and moment arm to account for the different sizes of the muscles. Total activation was defined as the sum of the agonist and antagonist muscle activities, while coactivation was defined as the minimum of the agonist and antagonist muscle activities (figure 9(A)). The second pair of indices was based on the torque produced by each musculotendon element (figure 9(B)). The total torque index was determined by the sum of the torques for agonists and antagonists, while cocontraction index was the minimum of

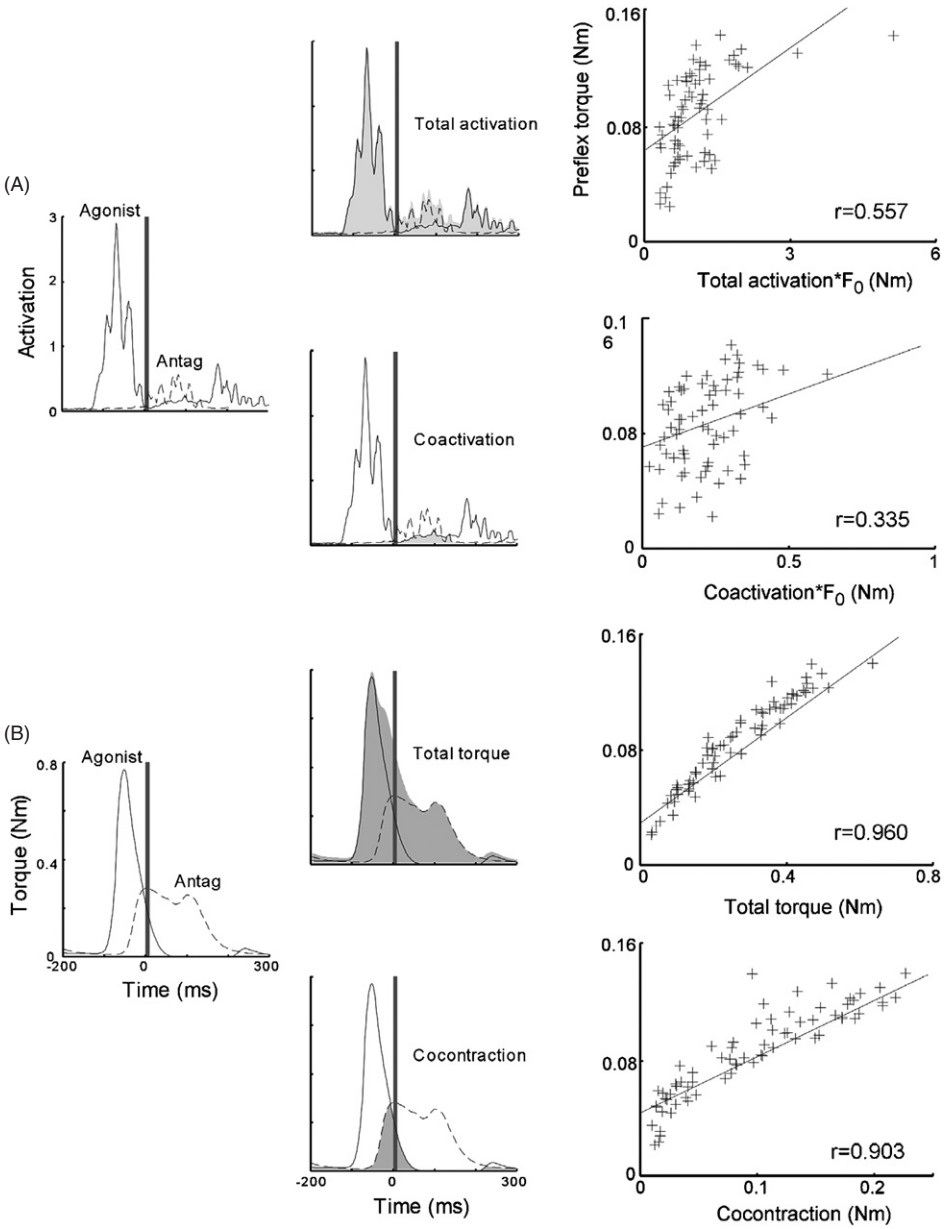

Figure 9. Four different muscle indices were computed to determine which correlated best with preflex impedance. (A) Two indices were based on the amount of activation used to drive the agonist (solid lines) and antagonist (dashed lines) muscle groups (scaled to the maximal isometric torque produced by each muscle according to calibration; see the materials and methods section). Total activation (the sum of agonist and antagonist activation) and coactivation (the minimum of the agonist or antagonist activation) are indicated by the shaded gray region in the middle column. In the right column, the values for the preflex epoch 10:20 ms after perturbation in each trial (indicated by dark gray bars in data traces) are plotted on the abscissa with the corresponding measured preflex torques on the ordinate. (B) Similar plots as in (A) but based on the total or minimal torque rather than activation. Two indices were based on the amount of muscle torque predicted during the simulated movement. These were quantified either as the total torque (i.e., sum of agonist and antagonist muscle torque) or cocontraction (i.e., minimum of the agonist and antagonist muscle torque). Total torque appeared to be the best predictor of preflex impedance, with correlation coefficient $r = 0.96$.

the agonist and antagonist torques. Best-fit linear regressions and their corresponding correlation coefficients (figure 9, right column) indicated that total torque was the best predictor of the magnitude of the preflex torque. This conforms to the simple mechanical explanation that the instantaneous impedance of the limb tends to be dominated by the force–velocity relationship of active muscle, which produces complementary and thus additive restorative force changes in both agonists and antagonists. It would be useful to extend this analysis for a wider range of perturbation magnitudes that would provide preflex torques that would be a larger percentage of total torque. This might also reveal whether the relationship is nonlinear, as suggested by the scatter plot based on total torque (figure 9(B)).

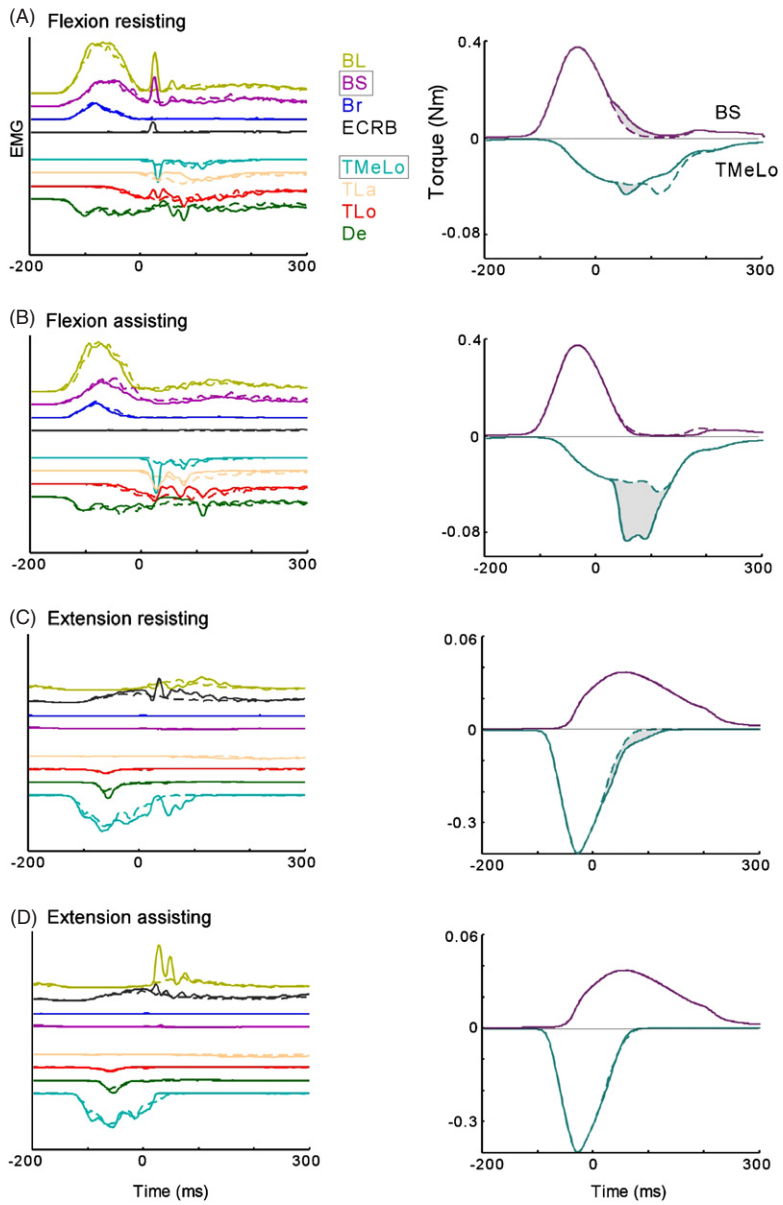

Figure 10. (A) Left column illustrates typical EMG data recorded from both unperturbed flexion-direction movements (solid line) and trials with resistive perturbations (dashed line) for the eight instrumented muscles. Reflexes appear as spikes or troughs in the EMG traces in perturbed trials (dashed line). Right column depicts torque predicted by musculoskeletal model with activation derived from perturbed (dashed line) and unperturbed (solid line) trials from BS and TMeLo. These muscles were selected because they showed the greatest amount of reflex activity. Other plots depict perturbed-condition EMG data derived from flexion-direction assistive perturbation trials (B), extension-direction resistive (C) and extension-direction assistive trials (D).

3.6. Use of reflexes to control perturbations (figure 10)

Typical reflex EMG responses to perturbations are shown in figure 10 (left column), averaged over all similar trials from a single session (flexor activity plotted upward, extensor downward). This muscle activity is typical of later sessions, when the torque pulse was stabilized at 1.62 Nm. EMG envelopes for the four different perturbation conditions are plotted (solid lines), superimposed over the EMG activity from unperturbed trials in the same session (dashed lines).

During the flexion task, resistive perturbations resulted in brief, large amplitude reflex responses in the flexors BL, BS and ECRB during the 10:30 ms (M1) interval. Interestingly, TLo, TLa and TMeLo antagonists also showed an increase in EMG activity during the same interval; however, this was followed by a period of about 50 ms when EMG activity was inhibited in the same muscles. The consequences of these reflexes on muscle torque are detailed in the right column for BS and TMeLo, the two muscles that had the strongest reflexes and the largest contributions to the corrective torques.

Flexion-direction trials with assistive perturbations (figure 10(B)) resulted in essentially no change in flexor muscle activity. Extensors TMeLo, TLa and to a lesser extent

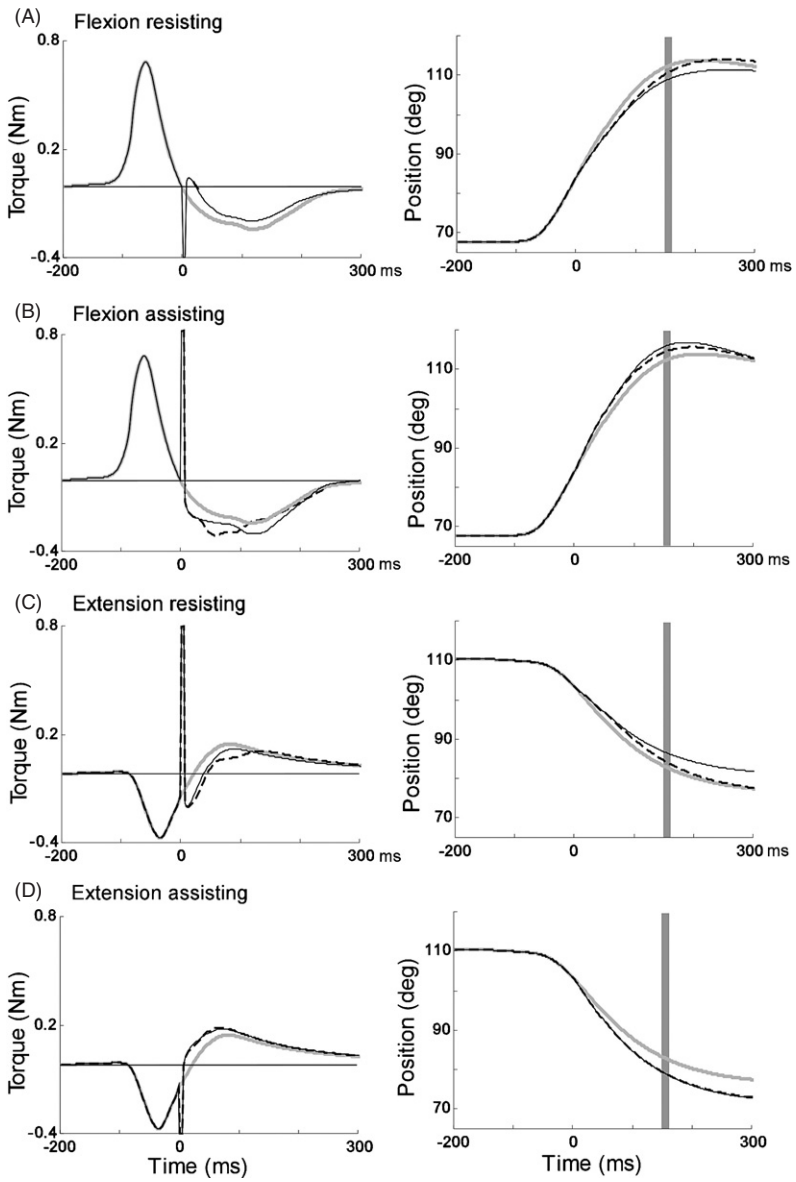

Figure 11. (A) Left column illustrates net muscle torque predicted by the model with activation derived from flexion-direction unperturbed trials which lack reflex components (solid line) or composite of unperturbed and perturbed trials (dashed line, see the materials and methods section) which include reflex components, in the presence of a resistive perturbation. The predicted nominal, unperturbed trajectory is depicted (thick gray line) for comparison. With reflex component included, there is initially a greater amount of torque immediately opposing the perturbation; later this situation reverses. Right column depicts the trajectories predicted in each of these three conditions. Error is measured as the deviation from the nominal trajectory at 150 ms, i.e. when the target window is entered (dark gray bar). The predicted error decreases when reflex components are included. Other plots are as above, but with activation data derived from (B) flexion-direction assistive perturbation trials or (C) extension-direction resistive and (D) extension-direction assistive trials.

TLo showed excitatory reflexes during the M1 interval, plus a second burst between 30:90 ms (M2). This resulted in a large increase in the braking torque predicted for TMeLo, which would counteract this perturbation.

The extension task was associated with less prominent reflexes in general. Resistive perturbations produced a long-lasting excitatory reflex in the extensor TMeLo at M2 latency, but the predicted torque effect was small (figure 10(C)). The flexor BL, which was cocontracting to provide braking torque, was inhibited, but ECRB (wrist extensor with weak elbow flexion moment) had M1 and M2 excitatory responses. Assistive perturbations produced strong short- and long-latency reflexes in BL only. BS participated only weakly as a brake on extension (EMG barely visible at this scale) and had no discernible reflexes.

3.7. Reflexive contribution to error correction following perturbations (figure 11)

The modeled reflex-induced changes in torque were examined to determine whether they were sufficient to affect movement

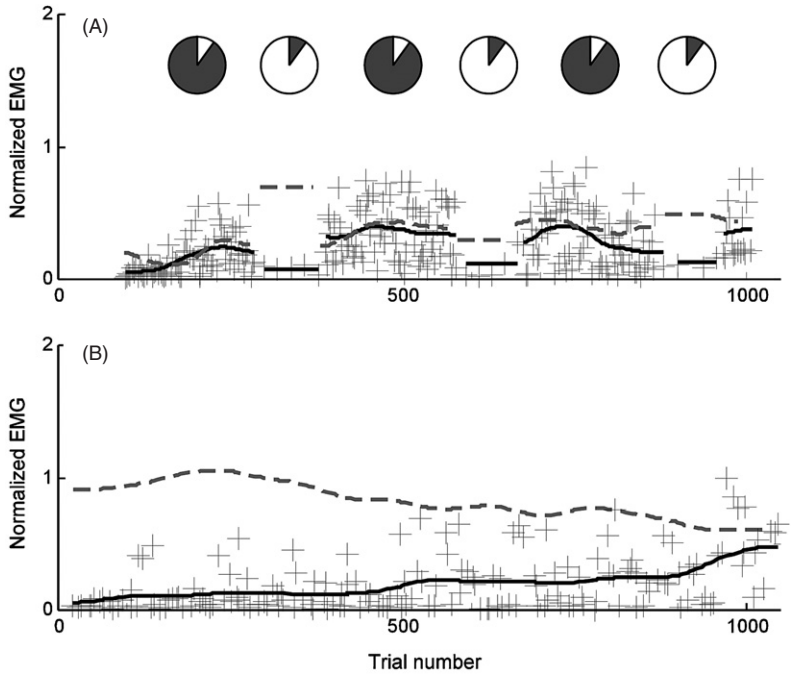

Figure 12. (A) Average amount of reflex activity in TMeLo in resistive trials only (crosses) in a single session versus trial number. Trend of reflex activity (solid black line), determined by a moving average window, is compared to trend of background activity (dashed gray line). Pie charts indicate the relative probability of each perturbation type used for each block of trials within the session; black indicates the proportion of resistive perturbations, gray indicates the assistive perturbations and white indicates the unperturbed trials. This session consisted of alternating blocks of 90% resistive/10% unperturbed and 10% resistive/90% unperturbed trials. Reflex activity was reduced in blocks of trials with fewer perturbations. (B) Reflex activity in a session consisting of equal amounts of each perturbation type. Reflex activity trended upwards over the session while background activity declined.

trajectory. Figure 11 depicts simulation trials where musculotendon elements were driven by EMG data from trials both with and without reflexes (see the materials and methods section). The net torque predicted during a resistively-perturbed flexion task is depicted in figure 11(A) (left column), which compares the torques with (dashed lines) and without (solid lines) the reflexive contributions to the nominal torque profiles without perturbation (gray lines). Both perturbed conditions result in the same corrective preflex torques, which can be seen immediately following the torque pulse. The reflexes produce an additional small but long-lasting corrective torque as well, starting about 30 ms after the end of the perturbation. The consequences of the perturbations and the preflex and reflex responses can be seen in the trajectories (right column). The position error at the time when the hand must be within the target window (vertical gray bar) is 3.44° (greater than the 3° target window) without reflexes and about half that with reflexes (1.75°).

The assistive perturbations during the flexion task (figure 11(B); error = −3.67° without reflexes versus −2.24° with reflexes) and the resistive perturbations during the extension task (figure 11(C); error = 3.61° versus 1.34°) both produced strong excitatory reflexes in TMeLo (figures 10(B) and (C)). These reflexes dominated the net torques and contributed substantially to reducing the trajectory error. In contrast, assistive perturbations during the extension task produced weak reflexes in all muscles (except the relatively weak BS; figure 10(D)) which had little effect on the perturbed trajectory (error = −3.87° versus −3.80°).

3.8. Independent modulation of background and reflexive activation (figure 12)

Increases in the background EMG activity of a muscle are likely to be associated with increases in reflex amplitudes simply because more motoneurons are already active or depolarized near threshold (Stein and Capaday 1988). In order to infer that reflex gain has been modulated by a 'gating' signal that does not affect motor recruitment directly, it is necessary to demonstrate that the reflex amplitudes do not covary simply with such background activity. We compared the pre-perturbation (non-reflex epoch defined in figure 4) and post-perturbation (reflex epoch) EMGs for TMeLo during the extension task with different probabilities of resistive perturbation. When only resistive perturbations were applied, sudden changes in the probability of such perturbations were accompanied by large and abrupt changes in both the background and reflex EMG that were often in opposite directions (figure 12(A)). In another session in which all the trials had equal probabilities of being unperturbed, resistively perturbed or assistively perturbed, the background activity gradually declined while the reflex amplitudes gradually increased (figure 12(B)). The significance of this observation must be tempered, however, by the problem noted post mortem with the placement of this electrode. It is possible that it

sampled from two separate motor pools (triceps medialis and triceps longus) that had different but constant reflex gains and that tended to be recruited differentially.

4. Discussion

Simulations are used only rarely to analyze experimental data from behavioral studies, probably because of the difficulty in specifying values for the many parameters of real musculoskeletal systems (Won and Hogan 1995, Smith and Humphrey 1991). In contrast, previous work (Loeb *et al* 1999) has considered the different properties of various levels of the neuromusculoskeletal hierarchy and demonstrated the usefulness of models for understanding their relative contributions, at least in highly simplified, model systems. The present study extends model-based analysis to a mechanically constrained but anatomically real preparation. We have combined realistic muscle morphometry measures with activation signals derived from recorded EMG in a *Macaca mulatta* performing a pointing task. The task itself was designed to evoke a rich set of adaptive changes in kinematic, muscle and reflex strategies in order to illustrate the utility of this model-based analysis. This paper presents results from only one animal, focusing on the utility of model-based analysis of such data rather than on the results themselves, which must be extended and confirmed in a larger study.

4.1. Evaluating muscle activity from recorded EMG

Well-constructed musculoskeletal models function as tools both to interpret the implications of behavioral observations and to identify potential limitations or sources of error in experimental techniques. A major goal of this study was to 'close the loop' on our EMG data and muscle models by determining if they could account for actual kinematic data. We attempted to record EMG signals from all of the muscles that could be involved in the task and predicted their torque contributions using a newly developed model of muscle activation that captures more of their recruitment and force dynamics than previously available models (Cheng *et al* 2000). The simple iterative method used here to identify best-fit gains for EMG to activation for each muscle can produce ambiguous results if a large set of values produces similarly good solutions. That situation is more likely to arise if the kinematic data set does not include a sufficiently broad range of behaviors that use different patterns of muscle synergy. In fact, the best-fit predictions of movement trajectories differed in some important respects from those recorded from the monkey, mooting the problem of ambiguity (see joint acceleration plots in figure 5(C), which reflect net effects of individual predicted muscle torques shown in figure 5(B)).

In order to determine whether the discrepancies in the kinematic output of the model reflected inadequacies in the EMG data or in the muscle model, we ran the model again using different muscle properties. Figure 13 compares the kinematics of the observed movements with those predicted to be produced by these monkey muscles when they were modeled with mechanical properties derived from cat and from human experiments. Unfortunately, there is little physiological data available from monkey muscles. We assumed that monkey muscles would probably have properties somewhere between the relatively fast cat muscles and the much slower human muscles (where speed refers both to rise and fall times of excitation–contraction coupling and to the ability to generate contractile force while shortening rapidly). The human muscle model reduced somewhat the large discrepancies during the agonist phase of the flexion task and perhaps during the antagonist phase of the extension task, both of which depend on the flexor muscles. However, qualitative discrepancies remained and the phases related to the extensor muscles started to show new discrepancies. This suggests that the source of these discrepancies lies in the EMG data or in the model of recruitment rather than in the values chosen to represent the physiological properties of the monkey muscles.

The most obvious source of error in EMG data would be failure to implant the correct muscles. This study employed more systematic methods than are usually employed in monkey behavioral studies, which often rely on percutaneous insertion of recording wires into only a subset of the muscles that could contribute to the task. The surgical errors that we discovered post mortem were surprising but at least they are known. It is interesting that even though we failed to implant properly the triceps medial head, an important extensor (Salmons 1995), the predicted extensorward accelerations accorded much better with actual acceleration data than did flexor accelerations, even though there were fewer overt problems with flexor muscle recordings. The likely reason is that EMG activity in an elbow extensor, TMeLo, appeared to be most representative of the activity of the entire muscle. There was a suggestion of this in the EMG signals before smoothing, which were less 'spiky' than those recorded in other muscles. EMG from TMeLo tended to be well defined, with consistent phasic bursts of activity as both an extension-direction agonist and a flexion-direction antagonist, and also in its clearly observed reflex activity (figure 10(A)). Conventional assessments based on signal-to-noise ratios and measures of electrode impedance, however, did not suggest any problems with the quality of the EMG data from any of the implanted muscles.

The kinematic discrepancies suggest that the EMG signals recorded from the flexor muscles did not accurately reflect the true activation of the entire muscle group. This problem may arise from the placement of recording electrodes in histochemically segregated portions of the muscles (Chanaud *et al* 1991) or in only one compartment of a muscle with neuromuscular compartmentation and differential recruitment (English and Weeks 1987). If the flexor muscle recordings happened to be made from relatively fast portions of the muscles, this would account for both the over-representation of the initial phases of flexorward acceleration and for the relatively spikey appearance of the raw EMG signals. Such a placement would record preferentially the activity of a small number of relatively large muscle units and would under-represent the contributions of smaller, slow-twitch units

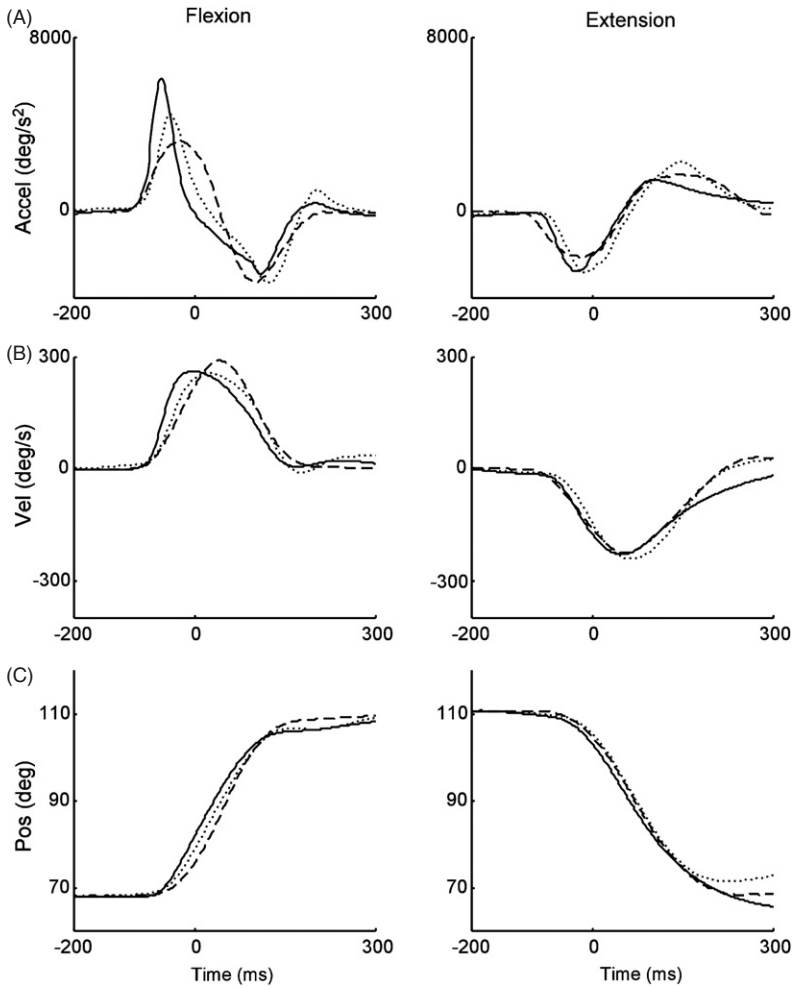

Figure 13. Predicted kinematics when musculotendon elements were given properties derived from feline (solid line) or human (dotted line) muscle fibers. Observed trajectories are displayed for comparison (dashed line). The model of feline slow-twitch muscle fibers had a contraction rise time of 30 ms (Kernell *et al* 1983) while human slow-twitch muscle fibers had a rise time of 65 ms (Desmedt and Godaux 1977). Kinematic data displayed are acceleration in degrees s^{-2} (A), velocity in degrees s^{-1} (B) and angular position in degrees (C).

that presumably account for the sustaining torque for the movement (Loeb and Gans 1986). Envelope extraction and averaging techniques such as employed here and in most such analyses (e.g., Angel (1975), Gottlieb (1996)) obscure such problems. This emphasizes the importance of understanding the underlying neuromuscular architecture of each muscle in order to determine the number and placement of EMG channels.

It is also possible that the kinematic discrepancies reflect a computational limitation of our implementation of the Virtual Muscle model. The version of Virtual Muscle available for this analysis made it impractical to construct muscle models with large numbers of separately recruitable motor units, so the models consisted of only a single slow-twitch motor unit. This results in an artificially abrupt recruitment curve that may have interfered with the ability to predict force output accurately. An improved version of Virtual Muscle that overcomes this limitation is now available (Song *et al* 2008b). Fortunately, many of the analyses described here are relatively unaffected by this discrepancy, whose existence and nature would have gone undetected without the method of 'closing the kinetic loop' to see if the recorded EMG activity actually accounts for the motor behavior.

4.2. Task differentiation of synergistic muscles

Contrary to the notion of 'lumping' synergistic muscles and muscle heads into single agonist or antagonist functional groups (Bouisset 1973), there were large and consistent differences in recruitment of muscles based on the task required of the muscles. These differences increased as the animal gained experience and skill at the task (figure 6(A)). By the final sessions in the data collection period, the ratio of EMG activity between action and braking roles for Br and BS was three to six times greater than that observed in BL. This particular monkey tended to recruit Br and BS almost exclusively during flexion acceleration of the forearm, while BL was preferred to brake extension motion. The energetic advantage of this specialization (figure 6(B)) suggests that this was an adaptive strategy learned by the animal. This

conclusion must be tempered, however, by the knowledge that the EMG signals available from the flexor muscles in this preparation had demonstrated sampling or modeling problems. If the slow-twitch motor units in these muscles were undersampled, it is possible that the specialization could reflect a departure from the size principle instead. The model-based analysis suggests that more systematic EMG sampling and more detailed modeling of these muscles will be necessary in order to support this attractive hypothesis.

The evolving specialization of muscle function with practice agrees with the notion that subjects attempt to reduce the complexity of a new task by reducing the number of degrees-of-freedom in the solution of the problem (e.g., by locking their joints or, in this case, by recruiting muscles synergistically; Bernstein 1967). Only when subjects become more proficient do they utilize more of the degrees-of-freedom actually available to the neuromuscular system, thereby achieving more accurate or efficient performance (McDonald *et al* 1989). Without a musculoskeletal model, or using musculoskeletal models that do not account for the specific moment arms and musculotendinous architecture of the individual muscles, we would have had no explanation for the differential recruitment of the elbow flexors in this task.

Lumping muscles into homogenously recruited 'muscle equivalents' (Bouisset 1973) is a simplification of the recruitment patterns observed behaviorally. This approach is commonly used when motor control models are developed (e.g., Osu and Gomi (1999), Karniel and Inbar (1997)). The question is whether such an approximation is justifiable; that is, whether the trade-off between simplicity and accuracy is deemed reasonable by the needs of the researcher. It is particularly important not to assume that such simplistic recruitment of synergistic muscles, whether recorded in a naive subject or assumed by a naive analysis, actually reflects an invariant CNS strategy for dealing with 'overcomplete' or 'redundant' musculature (Loeb 2000).

Differential recruitment of synergistic muscles in previous studies has been ascribed to their differential actions on other joints. For example, mono- and bi-articular arm muscles, such as brachioradialis and biceps brachii respectively, were found to be used to different degrees depending on the direction of hand movements (van Bolhuis *et al* 1998, van Bolhuis and Gielen 1997). In that case, the differential recruitment was attributed to the fact that brachioradialis is mono-articular, hence active only when an elbow flexion was required, irrespective of arm geometry or desired force direction. The biceps acts as both a shoulder and an elbow flexor, hence its activity was best correlated with the direction of hand movement, as opposed to any specific change in joint angle. The present study involved only a single degree-of-freedom movement, for which this explanation is inapplicable. This raises the question of whether the differential recruitment of bi-articular muscles was correctly attributed to articularity or might have arisen because of internal muscle architecture and the effects of kinematics on economy of force production.

Biomechanists often use anatomical origins and insertions to deduce the actions of individual muscles. Optimization criteria such as minimal muscle force (e.g., Seireg and Arvikar (1973)), minimal muscle stress (e.g., Crowninshield and Brand (1981)) or minimal energy consumption (e.g., Davy and Audu (1987)) are then applied to determine a pattern of activation that differentiates synergistic muscles. The EMG patterns obtained during a rich set of natural movements provide a much more direct indication of the motor strategies actually employed, which may not comport with such limited and arbitrary strategies.

4.3. Movement speed, impedance and energetics

The increase in movement speed over all sessions (figure 7(A)) was not explicitly required by the task, as time limits for the completion of the movement did not change between sessions. One possible reason is that faster movements are somehow more efficient and/or effective for coping with perturbations and the monkey learned this strategy over time. Previous research on skill acquisition suggests that skilled performers were able to make movements with greater efficiency as well as speed, as unnecessary movements and muscle activity declined (Sparrow 1983). In contrast, the musculoskeletal model indicated that the monkey actually did devote a greater amount of energy to the task during the later sessions (figure 8(B)).

Increasing movement speed, although energetically expensive, appears to be correlated with improved performance in the face of the brief torque perturbations used in these experiments. Simulations of the later, faster sessions proved to be less sensitive to torque pulses, resulting from the higher mechanical impedance in these movements (figure 8(C)). The impulse to the arm created by the torque pulse constitutes a smaller percentage of the momentum in the arm when it is moving at a higher velocity. Note that impulse (product of torque amplitude and duration) has the same units (N m s) as momentum (product of rotational inertia and velocity). The musculoskeletal model is useful for examining the effects of movement speed and muscle tone on impedance without the confounding effects of reflexes because it permits the application of the unperturbed EMG activity to the perturbed kinematics.

Higher velocities require higher torques to accelerate and decelerate the arm, requiring higher levels of muscle activity to achieve those torques. The intrinsic viscoelastic properties of active muscle result in instantaneous changes in contractile force when the length and the velocity of the muscle are changed such as by a perturbation. This reactive force has been called a 'preflex' because it is a zero-delay response that precedes even the shortest-latency reflexes (Brown *et al* 1995). Some studies associate increased preflexes with an increase in overall electromyographic activity (Lacquaniti *et al* 1982, Agarwal and Gottlieb 1977, Osu and Gomi 1999). Other studies focus on the mean level of muscular tension (Joyce and Rack 1969, Houk *et al* 1970) or the coactivation of antagonistic muscles (Hogan 1984) to explain the amount of mechanical impedance. The higher net muscle torques implied by higher accelerations do not necessarily translate into proportional changes in muscle activation because they could be achieved with more or less cocontraction of antagonists. In this light,

it is instructive to note that the preflex torque tended to be predicted best by the total torque produced by the muscles, not by the cocontraction component or by the weighted activation signals themselves (figure 9). In a dynamic task, EMG is not a good indicator of muscle impedance because of the large effects of velocity on active force generation.

Recently, the phenomenon of signal-dependent motor noise (Hamilton *et al* 2004) has been used to explain optimal control strategies that result in minimization of muscle force levels (Todorov 2004). The orderly but abrupt recruitment of motor units with a wide range of sizes causes higher levels of muscle force to be associated with larger random fluctuations in those forces. Under conditions where the kinematics result from the torques of synergistic muscles operating on passive loads such as inertia, such motor noise leads to kinematic variability. Under other conditions where antagonist muscles cocontract, their increased viscoelastic impedance at higher recruitment levels may counteract the higher motor noise (Selen *et al* 2005). The results presented here suggest that this viscoelastic impedance also provides advantages for dealing with externally applied perturbations and that the monkey perceived these advantages to be more important than any concomitant increase in motor noise. The recruitment model employed in this study did not include motor noise, but a newer version of Virtual Muscle (Song *et al* 2008b) can be driven so as to simulate motor noise.

While movement speed and levels of muscle recruitment and energy consumption increased over the entire training period, they tended to decrease within sessions (figure 7(B)). The simplest explanation, in the absence of any change in perturbation probability, is that the animal experienced fatigue over the course of the 1000 consecutive rapid arm movements. However, performance did not deteriorate, as might be expected. Instead, it appeared that the animal came to rely on more efficient use of reflexes (as demonstrated in figure 12(B); see below).

In a session comprising blocks of varied perturbation probabilities, the animal adjusted the peak acceleration depending on the frequency of each perturbation type (figure 7(C)). Blocks with a higher frequency of resistive trials tended to have higher peak acceleration and higher resultant peak velocity. This strategy is well suited to the nature of the target window. For example, consider the first block of 90% resistive/10% unperturbed trials. Essentially, the animal must initiate and terminate a ballistic movement within a window of $\pm 3^\circ$. With this perturbation schedule, the animal can make best use of the target window by deliberately overshooting the midpoint of the target by a few degrees. The resistive perturbation then tends to pull the hand back on target. Similarly, when a block consists of 90% assistive/10% unperturbed trials, deliberately undershooting the target would be a similarly adaptive strategy. This interpretation is supported by examining the angular position of the forearm at the time when the target window is first entered. Unperturbed trials sampled from the majority resistive blocks showed excursions 2–3° greater than those in the majority assistive blocks. This finding parallels strategies used by humans to cope with probabilistic targets (Favilla *et al* 1990, Ghez *et al* 1997).

4.4. The relative contribution of reflexes

Reflexes recorded in TMeLo were modulated according to the type of perturbation encountered (figure 12). These reflexes were modulated independently of background EMG activity, as has been observed in other studies (e.g., Johnson *et al* (1993), Dietz *et al* (1994)). The model-based analysis makes it possible to quantify the mechanical effects of the reflexes themselves, independent of the preflexive contributions of intrinsic muscle impedance. Furthermore, it permits those reflex contributions to be attributed to individual muscles, providing a link to the proprioceptive and spinal interneuronal circuits that presumably underlie those reflexes and their systematic and independent modulation. Such quantitative predictions must be tempered, however, by the possible effects of occlusion on gross EMG signals, which may be different for asynchronous voluntary activity versus more synchronous reflexive recruitment (Loeb and Gans 1986).

The specific results described and analyzed here likely depend on the limited range of experimental conditions explored in this single animal. Reflexes carried by oligosynaptic pathways are likely to exhibit threshold effects, so the absence of reflexes in many muscles under these relatively weak and brief torque pulses cannot be taken as an indication of the absence of reflexive projections. The delays inherent in reflexive responses mean that their utility will also depend on the timing of the perturbation during the course of the time-limited task. In addition to randomizing the sign and probability of occurrence of the perturbations, it would be useful to consider other magnitudes and timings of perturbations, but it is not clear that simply introducing them as additional randomizations would be appropriate. The gradual optimization of strategies (e.g. figure 6(A)) and the dependence of strategy selection on the perceived distribution of probability of occurrence of all perturbations (e.g. figures 7 and 12) all suggest that the monkey developed strategies based on maximizing probability of success across the totality of trials experienced. In unpublished experiments, we used a scaled-up version of the apparatus to deliver proportionately scaled perturbations to human subjects performing a similar task. They also adopted progressively more successful strategies that depended on probability distributions, but they reported paradoxically that they were unable to distinguish even the sign of such perturbations based on somatosensory information. For the type of task described herein, subjects appear to use visual feedback (which is available only after the end of the movement) for positive or negative reinforcement of strategies that are explored stochastically rather than analytically. For other types of perturbations such as continuous force fields, the nature of learning may be very different.

5. Conclusion

In motor control, the differentiation between intrinsic muscle stiffness and reflex stiffness (or, more correctly, impedance) is not a trivial one. It is the relative contribution of these two components that is central to the distinction between opposing

theories of equilibrium-point motor control (Asatryan and Feldman 1965, Bizzi *et al* 1978). Classical experiments have variously suggested that reflexes contribute significantly to stiffness (Sinkjaer and Hayashi 1989, Bennett 1994) or that they were only minimally effective (Allum 1975, Lacquaniti *et al* 1982, De Serres and Milner 1991). We suggest that accurate modeling studies can help to clarify some of the disagreement between these conflicting findings. Such models can identify limitations in design and shortcomings in execution of experiments and can reveal the quantitative mechanical implications of the kinematic and electromyographical data that are collected in behavioral experiments.

Acknowledgments

Experimental data were collected at Queen's University, Kingston, Canada, with the assistance of Ann Lablans. Current versions of the Virtual Muscle software used for the modeling can be downloaded from http://ami.usc.edu/projects/ami/projects/bion/musculoskeletal/

References

Agarwal G C and Gottlieb G L 1977 Compliance of the human ankle joint *J. Biomech. Eng.* **99** 166–70

Allum J H J 1975 Responses to load disturbances in human shoulder muscles the hypothesis that one component is a pulse test information signal *Exp. Brain Res.* **22** 307–26

Angel R W 1975 Myoelectric patterns associated with ballistic movement effect of unexpected changes in load *J. Hum. Mov. Stud.* **1** 96–103

Asatryan D G and Feldman A G 1965 Functional tuning of the nervous system with control of movement or maintenance of a steady posture: I. Mechanographic analysis of the work of the joint or execution of a postural task *Biofizika* **10** 837–46

Bak M J and Loeb G E 1979 A pulsed integrator for EMG analysis *Electroenceph. Clin. Neurophysiol.* **47** 738–41

Bennett D J 1994 Stretch reflex responses in the human elbow joint during a voluntary movement *J. Physiol. Lond.* **474** 339–51

Bennett D J, Gorassini M and Prochazka A 1994 Catching a ball contributions of intrinsic muscle stiffness reflexes and higher order responses *Can. J. Physiol. Pharm.* **72** 525–34

Bernstein N 1967 *The Coordination and Regulation of Movements* (London: Pergamon)

Bigland-Ritchie B, Johansson R, Lippold O C and Woods J J 1983 Contractile speed and EMG changes during fatigue of sustained maximal voluntary contractions *J. Neurophysiol.* **50** 313–24

Bizzi E, Dev P, Morasso P and Polit A 1978 Effects of load disturbances during centrally initiated movements *J. Neurophysiol.* **41** 542–56

Bouisset S 1973 EMG and muscle force in normal motor activities *New Developments in Electromyography and Clinical Neurophysiology* ed J E Desmedt (Basel: Karger) pp 547–83

Brown I E, Cheng E J and Loeb G E 1999 Measured and modeled properties of mammalian skeletal muscle: II. The effects of stimulus frequency on force–length and force–velocity relationships *J. Musc. Res. Cell Motil.* **20** 627–43

Brown I E, Liinamaa T L and Loeb G E 1996 Relationships between range of motion L0 and passive force in five strap-like muscles of the feline hind limb *J. Morphol.* **230** 69–77

Brown I E and Loeb G E 1999 Post-activation potentiation—a clue for simplifying models of muscle dynamics *Am. Zool.* **38** 743–54

Brown I E and Loeb G E 2000a Measured and modeled properties of mammalian skeletal muscle: IV. The dynamics of activation and deactivation *J. Musc. Res. Cell Motil.* **21** 33–47

Brown I E and Loeb G E 2000b A reductionist approach to creating and using neuromusculoskeletal models *Neuro-Control of Posture and Movement* ed J Winters and P Crago (New York: Springer) pp 148–63

Buchanan T S, Rovai G P and Rymer W Z 1989 Strategies for muscle activation during isometric torque generation at the human elbow *J. Neurophysiol.* **62** 1201–12

Chan S S and Moran D W 2006 Computational model of a primate arm: from hand position to joint angles, joint torques and muscle forces *J. Neural Eng.* **3** 327–37

Chanaud C M, Pratt C A and Loeb G E 1991 The roles of histochemical fiber-type regionalization and mechanical heterogeneity in differential muscle activation *Exp. Brain Res.* **85** 300–13

Cheng E J, Brown I E and Loeb G E 2000 Virtual Muscle: A computational approach to understanding the effects of muscle properties on motor control *J. Neurosci. Methods* **101** 117–30

Cheng E J and Scott S H 2000 Morphometry of *Macaca mulatta* forelimb: I. Shoulder and elbow muscles and segment inertial parameters *J. Morphol.* **245** 206–24

Collins J J 1995 The redundant nature of locomotor optimization laws *J. Biomech.* **28** 251–67

Crowninshield R D and Brand R A 1981 A physiologically based criterion of muscle force prediction in locomotion *J. Biomech.* **14** 793–801

Davy D T and Audu M L 1987 A dynamic optimization technique for predicting muscle forces in the swing phase of gait *J. Biomech.* **20** 187–201

De Serres S J and Milner T E 1991 Wrist muscle activation patterns and stiffness associated with stable and unstable mechanical loads *Exp. Brain Res.* **86** 451–8

Desmedt J E and Godaux E 1977 Ballistic contractions in man: characteristic recruitment pattern of single motor units of the tibialis anterior muscle *J. Physiol.* **264** 673–93

Dietz V, Discher M and Trippel M 1994 Task-dependent modulation of short- and long-latency electromyographic responses in upper limb muscles *Electroencephalogr. Clin. Neurophysiol.* **93** 49–56

English A W and Weeks O 1987 Anatomical and functional analysis of cat biceps femoris and semitendinosus muscles *J. Morphol.* **191** 161–75

Favilla M, Gordon J, Hening W and Ghez C 1990 Trajectory control in targeted force impulses. VII. Independent setting of amplitude and direction in response preparation *Exp. Brain Res.* **79** 530–8

Feldman A G, Ostry D J, Levin M F, Gribble P L and Mitinski A B 1998 Recent tests of the equilibrium-point hypothesis (lambda model) *Motor Control.* **2** 189–205

Georgopoulos A P 1986 On reaching *Annu. Rev. Neurosci.* **9** 147–70

Ghez C, Favilla M, Ghilardi M F, Gordon J, Mermejo R and Pullman S 1997 Discrete and continuous planning of hand movements and isometric force trajectories *Exp. Brain Res.* **115** 217–33

Goslow G E Jr, Cameron W E and Stuart D G 1977 Ankle flexor muscles in the cat: length-active tension and muscle unit properties as related to locomotion *J. Morphol.* **153** 23–37

Gottlieb G L 1996 On the voluntary movement of compliant (inertial-viscoelastic) loads by parcellated control mechanisms *J. Neurophysiol.* **76** 3207–29

Gottlieb G L 1998 Rejecting the equilibrium-point hypothesis *J. Motor Control.* **2** 10–12

Hamilton A, Jones K and Wolpert D 2004 The scaling of motor noise with muscle strength and motor unit number in humans *Exp. Brain Res.* **157** 417–30

Hays A V, Richmond B J and Optican L M 1982 A UNIX-based multiple process system for real-time data acquisition and control *WESCON Conf. Proc.* **2** 1–10

Hogan N 1984 Adaptive control of mechanical impedance by co-activation of antagonist muscles *IEEE Trans. Autom. Control* **29** 681–90
Houk J C, Singer J J and Goldman M R 1970 An evaluation of length and force feedback to soleus muscles of decerebrate cats *J. Neurophysiol.* **3** 784–811
Jaric S, Gottlieb G L, Latash M L and Corcos D M 1998 Changes in the symmetry of rapid movements: effects of velocity and viscosity *Exp. Brain Res.* **120** 52–60
Johnson M T V, Kipnis A N, Lee M C and Ebner T J 1993 Independent control of reflex and volitional EMG modulation during sinusoidal pursuit tracking in humans *Exp. Brain Res.* **96** 347–62
Joyce G C and Rack P M H 1969 Isotonic lengthening and shortening movements of cat soleus muscle *J. Physiol. Lond.* **204** 475–91
Karniel A and Inbar G F 1997 A model for learning human reaching movements *Biol. Cybern.* **77** 173–83
Kaufman K R, An K-N, Litchy W J and Chao E Y S 1991 Physiological prediction for muscle forces: I. Application to isokinetic exercise *Neuroscience* **40** 793–804
Kernell D, Eerbeek O and Verhey B A 1983 Relation between isometric force and stimulus rate in cat's hindlimb motor units of different contraction times *Exp. Brain Res.* **50** 220–7
Lacquaniti F, Licata F and Soechting J F 1982 The mechanical behavior of the human forearm in response to transient perturbations *Biol. Cybern.* **44** 35–46
Lee R G and Tatton W G 1975 Motor responses to sudden limb displacements in primates with specific CNS lesions and in human patients with motor system disorders *Can. J. Neurol. Sci.* **2** 285–93
Lee R G and Tatton W G 1982 Long latency reflexes to imposed displacements of the human wrist: dependence on duration of movement *Exp. Brain Res.* **45** 207–16
Loeb G E 2000 Overcomplete musculature or underspecified tasks? *Motor Control* **4** 81–3
Loeb G E and Gans C 1986 *Electromyography for Experimentalists* (Chicago: University of Chicago Press)
Loeb G E, Brown I E and Cheng E J 1999 A hierarchical foundation for models of sensorimotor control *Exp. Brain Res.* **126** 1–18
Marsden C D, Merton P A and Morton H B 1972 Servo action in human voluntary movement *Nature* **238** 140–43
McDonald P V, van Emmerick R E and Newell K M 1989 The effects of practice on limb kinematics in a throwing task *J. Motor Behav.* **21** 245–64
Nakazawa K, Yamamoto S-I and Yano H 1997 Short- and long-latency reflex responses during different motor tasks in elbow flexor muscles *Exp. Brain Res.* **116** 20–28
Osu R and Gomi H 1999 Multijoint muscle regulation mechanisms examined by measured human arm stiffness and EMG signals *J. Neurophysiol.* **81** 1458–68
Pigeon P, Yahia L'H and Feldman A G 1996 Moment arms and lengths of human upper limb muscles as functions of joint angles *J. Biomech.* **29** 1365–70
Salmons S 1995 Muscle *Gray's Anatomy* 38th edn ed L H Bannister, M M Berry, P Collins, M Dyson, J E Dussek and M W J Ferguson (New York: Churchill Livingstone) pp 737–900
Schutte L M, Rodgers M M and Zajac F E 1993 Improving the efficacy of electrical stimulation-induced leg cycle ergometry: an analysis based on a dynamic musculoskeletal model *IEEE Trans. Rehabil. Eng.* **1** 109–25
Scott S H and Loeb G E 1995 Mechanical properties of the aponeurosis and tendon of the cat soleus muscle during whole-muscle isometric contractions *J. Morphol.* **230** 69–77
Seireg A and Arvikar R J 1973 A mathematical model for evaluation of forces in lower extremities of the musculoskeletal system *J. Biomech.* **6** 313–26
Selen L P J, Beek P J and van Dieen J H 2005 Can co-activation reduce kinematic variability? A simulation study *Biol. Cyber.* **93** 373–81
Sinkjaer T and Hayashi R 1989 Regulation of wrist stiffness by the stretch reflex *J. Biomech.* **22** 1133–40
Smith A M and Humphrey D R 1991 What do studies of specific motor acts such as reaching and grasping tell us about the general principles of goal-directed motor behavior? *Motor Control: Concepts and Issues* ed D R Humphrey and H J Freund (New York: Wiley) pp 357–81
Soechting J F and Flanders M 1997 Evaluating an integrated musculoskeletal model of the human arm *J. Biomech. Eng.* **119** 93–102
Song D, Lan N, Loeb G E and Gordon J 2008a Model-based sensorimotor integration for multi-joint control—development of a virtual arm model *Ann. Biomed. Eng.* **36** 1033–48
Song D, Raphael G, Lan N and Loeb G E 2008b Computationally efficient models of neuromuscular recruitment and mechanics *J. Neural Eng.* **5** 175–84
Sparrow W A 1983 The efficiency of skilled performance *J. Motor Behav.* **15** 237–61
Stein R B and Capaday C 1988 The modulation of human reflexes during functional motor tasks *Trends Neurosci.* **11** 328–32
Todorov E 2000 Direct cortical control of muscle activation in voluntary arm movements: a model *Nature Neurosci.* **3** 391–8
Todorov E 2004 Optimality principles in sensorimotor control *Nature Neurosci.* **7** 907–15
van Bolhuis B M and Gielen C C 1997 The relative activation of elbow-flexor muscles in isometric flexion and flexion/extension movements *J. Biomech.* **30** 803–11
van Bolhuis B M, Gielen C C and van Ingen Schenau G J 1998 Activation patterns of mono- and bi-articular arm muscles as a function of force and movement direction of the wrist in humans *J. Physiol.* **508** 313–24
van der Helm F C T 1994 Analysis of the kinematic and dynamic behavior of the shoulder mechanism *J. Biomech.* **27** 527–50
Veeger H E J, Yu B, An K and Rozendal R H 1997 Parameters for modeling the upper extremity *J. Biomech.* **30** 647–52
Wolpaw J R, Maniccia D M and Elia T 1994 Operant conditioning of primate H-reflex: phases of development *Neurosci. Lett.* **170** 203–7
Won J and Hogan N 1995 Stability properties of human reaching movements *Exp. Brain Res.* **107** 125–36
Yamamoto C and Ohtsuki T 1989 Modulation of stretch reflex by anticipation of the stimulus through visual information *Exp. Brain Res.* **77** 12–22
Zajac F E 1989 Muscle and tendon: properties, models, scaling and application to biomechanics and motor control *Crit. Rev. Biomed. Eng.* **17** 359–411